CHAPTER # 3

CATALYST CHARACTERIZATION

3.1 INTRODUCTION

The characterization of a catalyst is an important part of catalytic research and development programme. Now-a-days novel techniques and sophisticated instruments are used to characterize the catalyst structure before, during and after the use. These development have resulted in a better understanding of the catalytic phenomena. The application of advanced electronics and computer analysis has optimized many of these analytical tools. Thus, the difficult goal of unravelling the relationship between the structure and reactivity of catalytic materials is finally within the reach. However the complete characterization of the supported catalyst is extremely difficult due to inhomogeneous nature of the catalyst themselves. Accordingly, a wide range of analytical and spectroscopic techniques have been applied to the problem(1,2).

The characterization of a catalyst provides information on three distinct but related sorts. These are : chemical composition and structure, texture and mechanical properties and catalytic activity.

Chemical composition and chemical structure refer to the elemental composition, proportions of individual phase present, surface composition, nature and properties of surface functional groups. The structure of a catalyst referes to its geometric structure and morphology. The characterization of a catalyst in terms of its activity is a quantitative measure of the ability of the catalyst to carryout a perticular chemical transformation under specified condition.

A typical characterization procedure would involve a careful record of the conditions under which the supported catalyst had been prepared, microanalysis for as many of the elements present and application of spectroscopic techniques to study the response of the supported catalyst to probe molecules such as carbon-monoxide, hydrogen and nitric oxide. All the approaches put together help to arrive at the possible structure of the metal complex on the polymer.

Present chapter deals with the physico-chemical characterization of polymer bound complexes such as chemical composition, moisture content, apparent bulk density, surface area and swelling studies. Spectroscopic studies have been utilized to investigate the coordination structure of polymer supported metal complexes, oxidation state of metal atom and crystallinity of the supported complexes using techniques such as UV-Vis, IR, FTIR, ESR and SEM. Thermal stability of the support and supported catalysts has been studied by the use of DTA and TG analysis. Based on the spectroscopic and physico-chemical characteristics the probable structures of the metal complexes have been proposed on polymer matrices as shown in scheme 3.1.

3.2 APPARENT BULK DENSITY AND MOISTURE CONTENT

The apparent bulk density is an important practical parameter because it indicates the mass of catalyst which is packed into a reactor of specified volume. When the polymer supported catalyst is employed in a liquid phase slurry reactor, the apparent bulk density may not play a significant role because of the higher volume occupied by swollen polymer than

the dry polymer as also the swelling capacity differs from solvent to solvent.

Apparent bulk density and moisture content of all the catalysts are given in Table 3.1. Apparent bulk density and percent moisture content of the catalysts were found to increase with an increase in percent crosslinking of the polymer support. Since the polymer (poly styrene-divinyl benzene) support is hydrophobic in nature (3), the similar nature of the supported catalysts may be attributed either due to hydrogen bonding of water with amino groups or coordination with metal atom.

3.3 CHEMICAL COMPOSITION

Elemental analysis of carbon, hydrogen, nitrogen and metal content of ruthenium and palladium complexes of 2 - amino butanol and glycine at various stages are given in Tables 3.2 - 3.3; the calculated and experimental values were found to be in close agreement. The loading of the metal ions was found to be poor. The chelation on the polymer matrix was achieved by carrying out the complexation under mild condition using good swelling agent.

In general, the formation of the metal complex on the surface of polymer represents a complicated process. The polymer matrix swells after absorbing the solvent which changes the polymer structure. The swollen polymer then interacts with metal ions and forms the complex. It may be taken into account that each functional group comes in contact with metal ions and co-ordinates with polymer to form " inner coordination complex ". Then the special arrangement of the

TABLE 3.1

Apparent bulk density and moisture content of polymer supported catalysts

Catalyst	Moisture Content (Wt%)	Apparent Bulk density ($g.cm^{-3}$)
2P[Ru(L2AB)Cl_3]	1.75	0.425
2P[Pd(L2AB)Cl_2]	1.32	0.423
2P[Ru(Gly)Cl_3]	1.61	0.382
8P[Ru(L2AB)Cl_3]	2.96	0.475
8P[Ru(Gly)Cl_3]	2.23	0.480
8P[Pd(L2AB)Cl_2]	3.85	0.476
8P[Pd(Gly)Cl_2]	2.25	0.482
14P[Pd(L2AB)Cl_2]	3.86	0.488
14P[Pd(Gly)Cl_2]	3.49	0.498

Table 3.2 Elemental analyis and metal loading at different stages of reaction for polymer bound ruthenium catalysts in (wt%)

CATALYST	P			Q			R			
	C	H	Cl	C	H	N	C	H	N	Ru (g/g)
A	80.94	7.46	6.00	84.68	8.26	1.23	87.40	8.18	1.12	3.21×10^{-4}
B	80.94	7.46	6.00	86.36	6.77	1.08	87.45	6.71	< 1	4.50×10^{-4}
C	72.95	5.93	17.50	85.88	7.19	3.68	87.90	6.33	3.32	3.25×10^{-4}
D	72.95	5.93	17.50	85.76	5.96	2.01	87.22	5.66	1.82	6.75×10^{-4}

P : After Chloromethylation

Q : After Ligand insertion

R : After Complex formation

A: 2P[Ru(L2AB)Cl_3]

B: 2P[Ru(Gly)Cl_3]

C: 8P[Ru(L2AB)Cl_3]

D: 8P[Ru(Gly)Cl_3]

Table 3.3 Elemental analyis and metal loading at different stages of reaction for polymer bound palladium catalysts in (wt%)

CATALYST	P			Q			R			
	C	H	Cl	C	H	N	C	H	N	Pd (g/g)
E	80.94	7.46	6.00	84.68	8.26	1.23	85.11	7.34	1.12	5.50×10^{-4}
F	72.95	5.93	17.50	85.88	7.19	3.68	85.63	7.09	3.26	2.75×10^{-4}
G	72.95	5.93	17.50	78.50	7.16	2.00	78.35	6.15	1.74	6.25×10^{-4}
H	83.84	8.40	4.70	86.52	8.90	2.72	85.76	8.84	2.17	5.44×10^{-4}
I	83.84	8.40	4.70	86.70	9.20	1.14	86.40	9.10	< 1	6.19×10^{-4}

P : After Chloromethylation

Q : After Ligand insertion

R : After Complex formation

E : 2P[$Pd(L2AB)Cl_2$]

F : 8P[$Pd(L2AB)Cl_2$]

G : 8P[$Pd(Gly)Cl_2$]

H : 14P[$Pd(L2AB)Cl_2$]

I : 14P[$Pd(Gly)Cl_2$]

complexing groups over the polymer ligand chain takes various orientations with respect to the main chain. As a result, the total polymer complex as a whole is formed. The polymer complex formation also represents a relaxation process, which is related to the probability of transition of the system from one state to another via equilibrium.

3.4 SURFACE AREA MEASUREMENT

The measurement of total surface area of the supports and supported catalysts were carried out using non-specific physical adsorption method (4,5). Adsorption-desorption isotherms of nitrogen were measured using carlo-Erba sorptomatic series-1900 at 196°C (liquid-nitrogen temperature) after degassing the sample at 80°C for four hours. From the isotherms specific surface area and pore volume were calculated using BET equation. The surface area and pore volume of the supports and supported catalysts are given in Tables 3.4 & 3.5 respectively. A change in surface area was observed in all the cases. The reduction in surface area of 2% support was found to be large while in case of 8% and 14% supports a small change was observed in surface area after anchoring of the complexes. The decrease observed in the surface area could be due to blocking of pores of the support by the successive introduction of chloromethyl group, ligand and formation of metal complex on the surface of the support.

3.5 SWELLING STUDIES

In order to optimise the rate and specificity both of a particular catalyst system, it is necessary to consider many factors. The nature of the solvent used plays an important

TABLE 3.4

The surface area and pore volume of supports.

Support	Surface Area ($m^2 . g^{-1}$)	Pore Volume ($cm^3 . g^{-1}$)
2P	330.00	0.420
8P	37.37	0.04
14P	62.03	0.07

TABLE 3.5

Surface area and pore volume of supported catalysts

Catalyst	Surface Area ($m^2 . g^{-1}$)	Pore Volume ($cm^3 . g^{-1}$)
2P[Ru(L2AB)Cl_3]	203.39	0.59
2P[Pd(L2AB)Cl_2]	174.17	0.36
2P[Ru(Gly.)Cl_3]	243.25	0.65
8P[Ru(L2AB)Cl_3]	34.70	0.15
8P[Ru(Gly.)Cl_3]	40.40	0.08
8P[Pd(L2AB)Cl_2]	33.95	0.08
8P[Pd(Gly.)Cl_2]	27.00	0.06
14P[Pd(L2AB)Cl_2]	63.38	0.33
14P[Pd(Gly.)Cl_2]	73.03	0.26

role in the rate of reaction. Swelling of polymer beads is a very useful parameter to control both specificity and selectivity in a batch reactor.

To achieve the higher activity and selectivity with polymer bound catalysts, it is necessary that the reactant molecules have accessibility to all catalytic sites both on the surface and the interior of the beads. This requires the use of a suitable solvent in which the polymer has a maximum swelling so that the matrix expands sufficiently to allow the reactant molecules to diffuse within the solvent channel and encounter the catalytic site.

The extent of swelling depends on the polymer-solvent interaction which is determined not only by the nature of solvent and the polymer matrix but also by the active groups attached to the polymer matrix.

An exhaustive swelling studies were carried out for supports and the supported catalysts using ten different solvents of various nature (i.e. polar and non-polar). A change in swelling was observed for different solvents when the ligands as well as the metal ions were incorporated on the surface of the polymer matrix. Non-polar solvents were found to be poor swelling agent, whereas polar solvents have a maximum swelling capacity. The results are given in Tables 3.6 and 3.7. A higher swelling was found in case of water which might be due to the intermolecular H-bonding between amino groups and water molecules. However, methanol was chosen as the reaction medium because of the good swelling agent for the catalysts as well as the higher solubility of the substrate.

TABLE 3.6

Swelling studies of polymer supports in different solvents (mol %)

Solvent	2% support	8% support	14% supports
Water	4.03	3.83	4.20
Methanol	3.12	2.52	2.30
Ethanol	2.30	1.81	1.78
Dioxane	1.84	1.42	1.32
DMF	1.52	1.27	1.13
Acetone	1.37	1.10	1.02
THF	1.06	1.00	0.91
Benzene	1.00	0.83	0.78
Cyclohexane	0.88	0.68	0.57
n-heptane	0.73	0.52	0.48

Table 3 7 Swelling studies of polymer bound catalysts in different solvents (Mole %)

catalyst / solvent	A	B	C	D	E	F	G	H	I
Water	3 61	4.91	3 73	3.71	4 12	4 08	2 73	3 98	2.70
Methanol	2 85	1.40	2.36	1.83	1 91	1.90	2.03	1.65	1.98
Ethanol	1 83	1.20	1.50	1 35	1 45	1 44	1.50	1 41	1.43
Dioxane	1.36	1.01	1 15	1.23	1 01	0.81	1.15	0.76	1.11
DMF	1.24	1.00	1.00	1.14	0 88	0.67	1.00	0.61	0.97
Acetone	1.01	0.98	0.91	0 96	1.05	0.93	0.91	0.58	0.83
THF	0 92	0.90	0.90	0 85	0 92	0.85	0.90	0.54	0.79
Benzene	0.91	0.81	0.74	0.64	0.93	0.75	0.74	0.50	0.70
Cyclohexane	0.52	0.73	0.44	0.48	0.70	0.54	0 44	0.42	0.41
n-heptane	0.44	0.67	0.41	0 36	0 44	0.38	0.41	0.31	0.36

Where, A: 2P[Ru(L2AB)Cl_3] E : 2P[Pd(L2AB)Cl_2]

B: 2P[Ru(Gly)Cl_3] F . 8P[Pd(L2AB)Cl_2]

C: 8P[Ru(L2AB)Cl_3] G : 8P[Pd(Gly)Cl_2]

D: 8P[Ru(Gly)Cl_3] H . 14P[Pd(L2AB)Cl_2]

I : 14P[Pd(Gly)Cl_2]

3.6 SPECTRAL CHARACTERIZATION

3.6.1 UV-VISIBLE SPECTROSCOPY

The interaction of light with catalyst particles is a major tool for the characterization of the catalysts. The transitions involved in UV-visible region are electronic. Thus, d-d transitions are observed when degenerate d-orbitals split by placing a transition metal ion in a crystal field. The splitting of the energy level is affected by the number of d-electrons, the effective charge on the ion, the distribution and the charge of the surrounding ions. These transitions usually occur in the visible part of the spectrum. Charge transfer transitions involve more than one atom and include transitions from metal to ligand or vice versa or between two neighbouring metal atoms of different oxidation states. Usually such transitions occur in the UV region and do not mask the d-d transitions in the visible region. The technique employed in UV-visible spectroscopy for powdered samples involves the measurement of diffusely reflected light (6,7). Figs. 3.1 and 3.2 show the UV-visible diffuse reflectance spectra recorded for polymer bound ruthenium and palladium complexes using $BaSO_4$ as standard.

In case of polymer bound ruthenium complexes a broad absorption band between 350 and 390 nm was assigned due to d-d transition of Ru(III) and for palladium (II), the absorption bands appeared between 376 and 387 nm.

Fig. 3.3 shows the UV-visible spectra of unbound catalyst. The presence of 3 bands observed at 436, 332 and 324 nm is because of Pd(II) d^8 metal ion and there are three

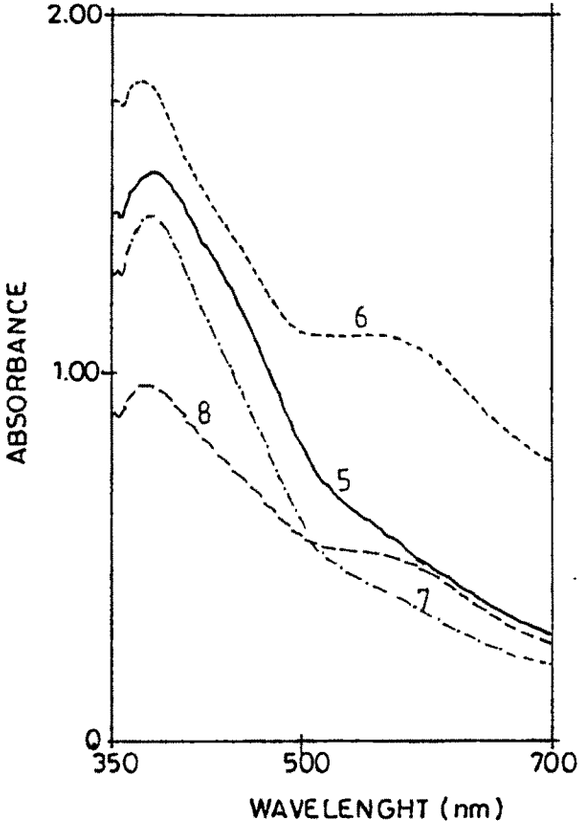

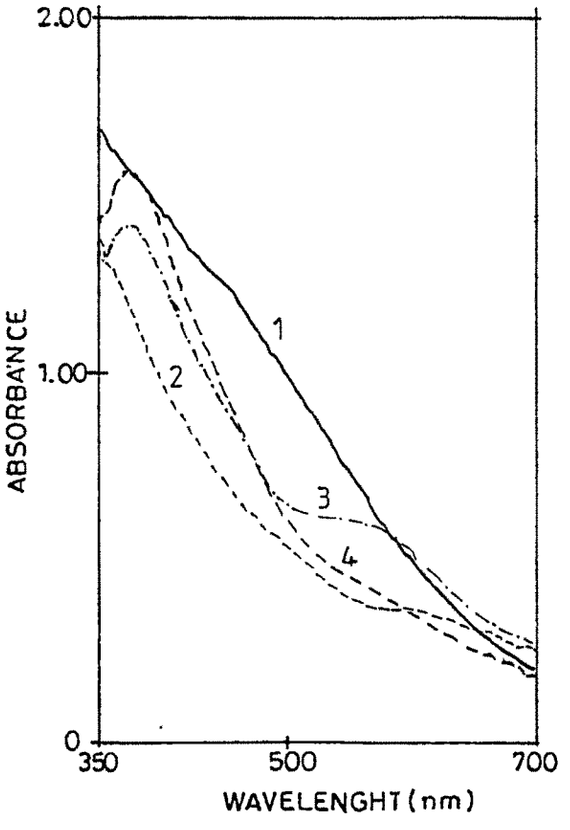

FIG. 3.1 UV-VIS reflectance spectra of

(1) 2P[Pd(L2AB)Cl_2] (2) 2P[Ru(L2AB)Cl_3] (3) 8P[Pd(L2AB)Cl_2]
(4) 8P[Ru(L2AB)Cl_3] (5) 14P[Pd(L2AB)Cl_2] (6) 14P[Pd(Gly)Cl_2]
(7) 8P[Ru(Gly)Cl_3] (8) 8P[Pd(Gly)Cl_2]

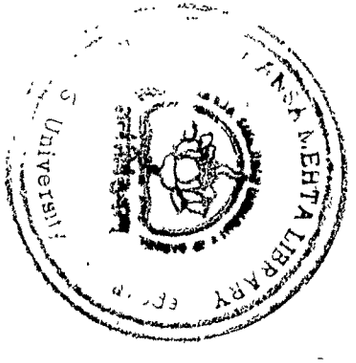

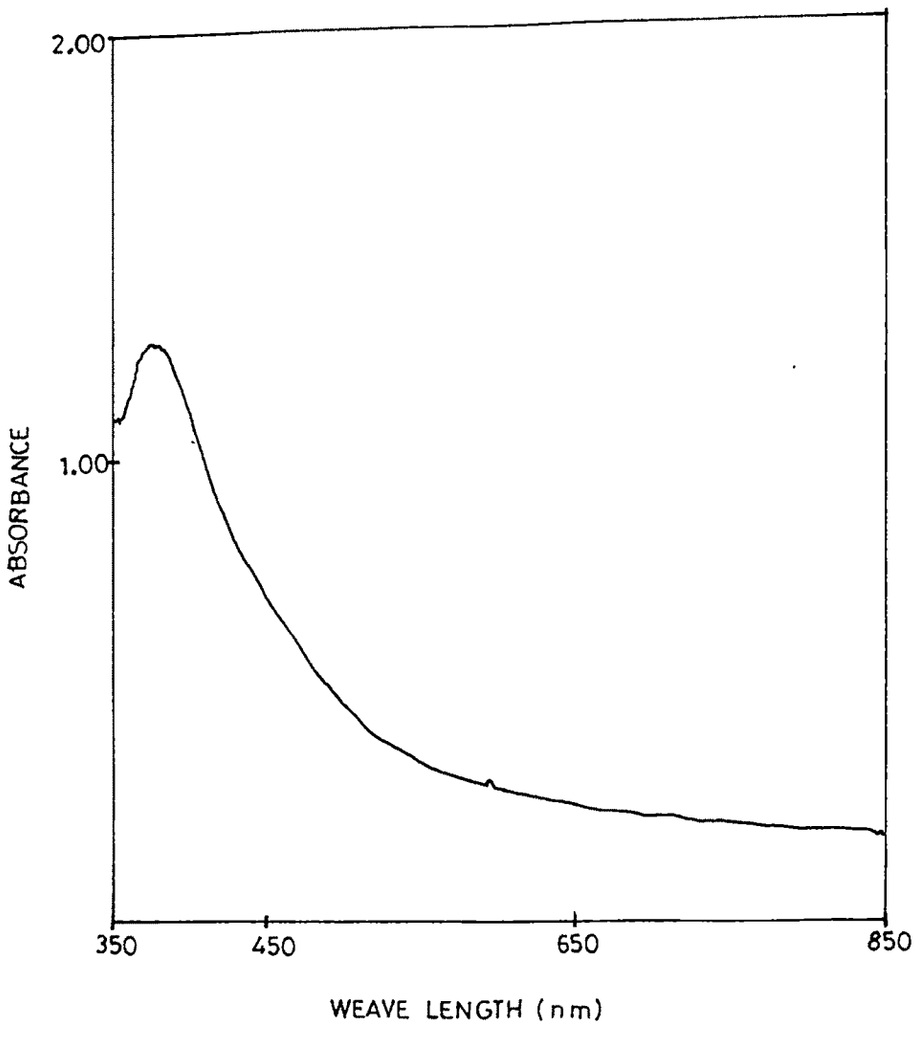

FIG: 3.2 UV-VIS reflectance spectra of (9) 2P[$Ru(Gly)Cl_3$]

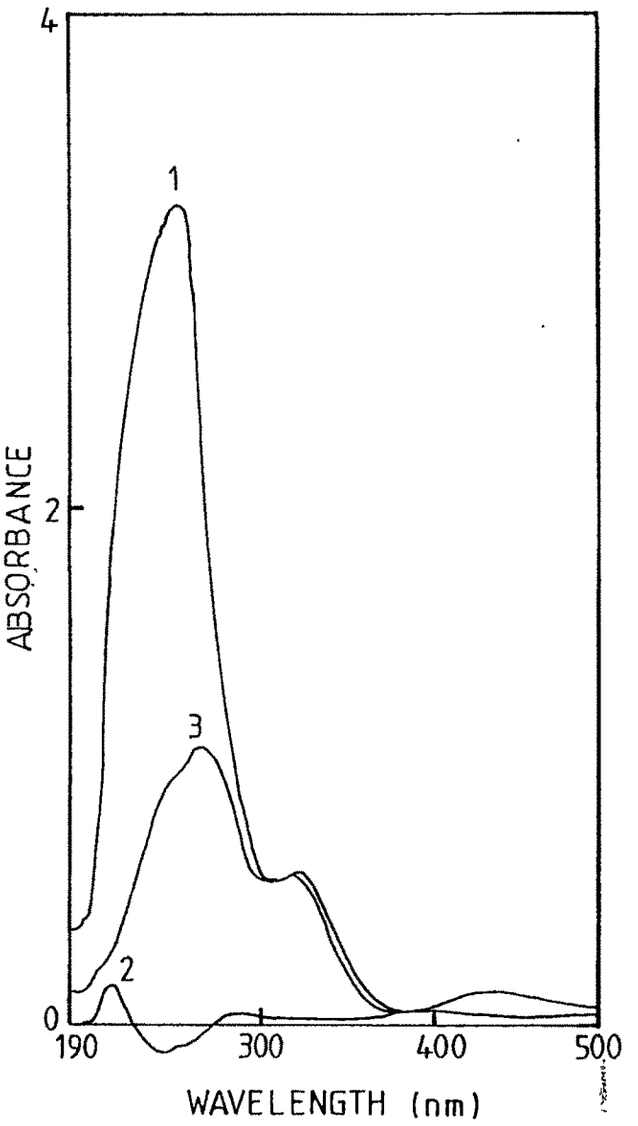

Fig. 3.3 UV-VIS absorbance spectrum of (1) $PdCl_2$ (2) L-2-Aminobutanol (3) [Pd(L2AB)Cl_2]

transitions possible within the 4d electronic level Band observed at 436 nm is very broad and hence any change in position due to change in crystal field created by 2-amino butanol is not significant However, the bands at 332 nm and 324 nm position are observed to undergo a shift of 8 nm in the solution containing 2-amino butanol The shift in position clearly indicates the formation of metal complex in homogeneous system

3.6.2 INFRARED SPECTROSCOPY

Generally infrared spectroscopy has been used for characterization of organometallic compounds It provides reliable information about the organic compounds in the IR (i.e 600-4000cm^{-1}) region and that of metal ligand vibrations in Far-IR (50– 600 cm^{-1}) region The formation of metal complex on polymer support after attachment of functional group, ligand molecule and metal ion can be understood by the nature and position of the absorption bands (8,9).

Absorption spectra of polymer bound ligands or metal ions are changed some times drastically by complex formation Since in a polymer bound metal complex, a huge macromolecular chain is adjacent to the coordinating group influences the absorption band in the spectra Hence the spectra will be dependent on the nature of the polymer chain (10).

Infrared spectra of polymer anchored catalysts are given in Figs 3.4 to 3.9. The IR absorption frequency of a ligand is usually shifted by complex formation with metal atom (11,12) A summary of the IR frequency assignment for all the catalysts

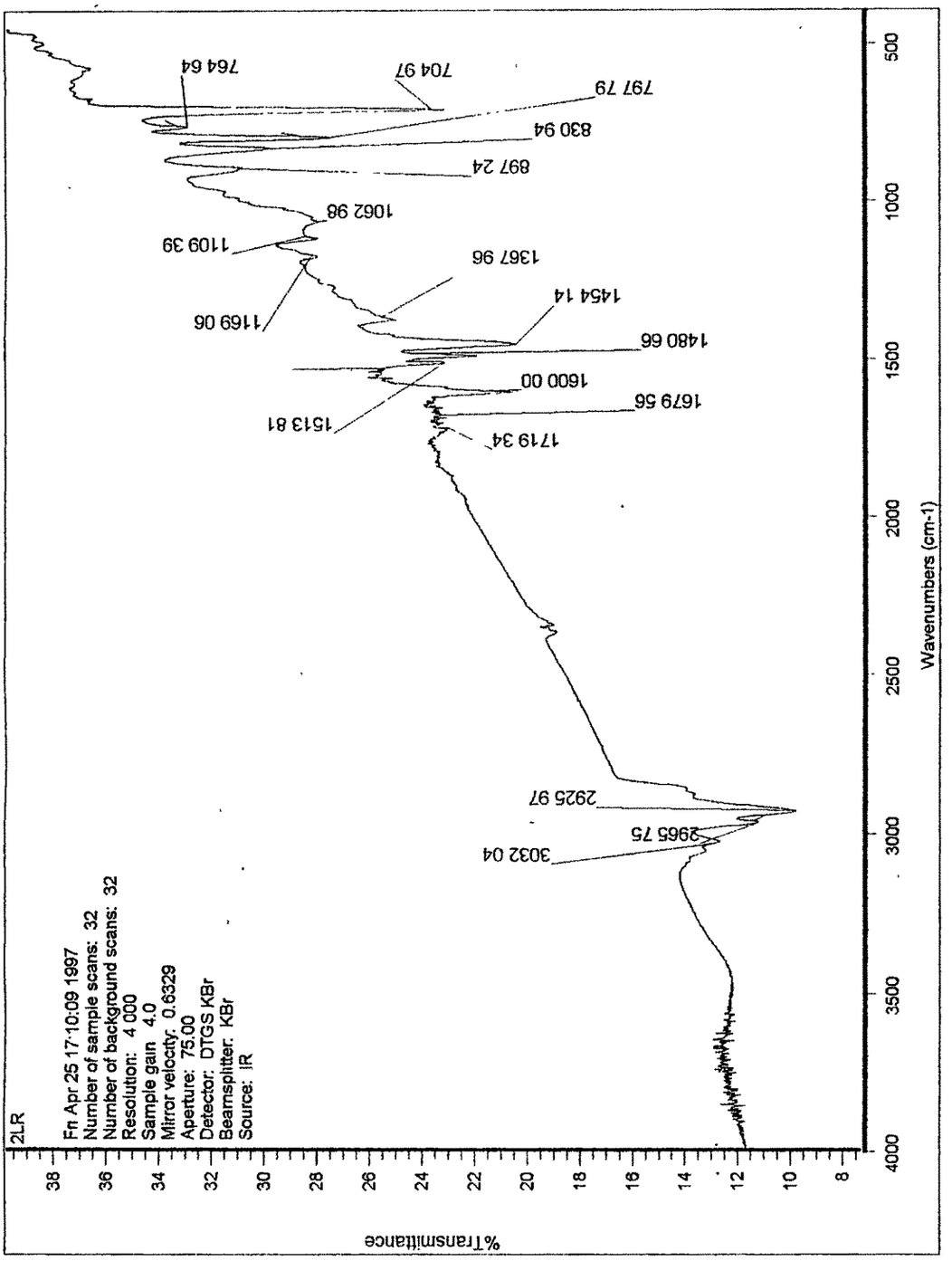

FIG 3 4 Infrared spectra of 2P[Ru(L2AB)Cl_3]

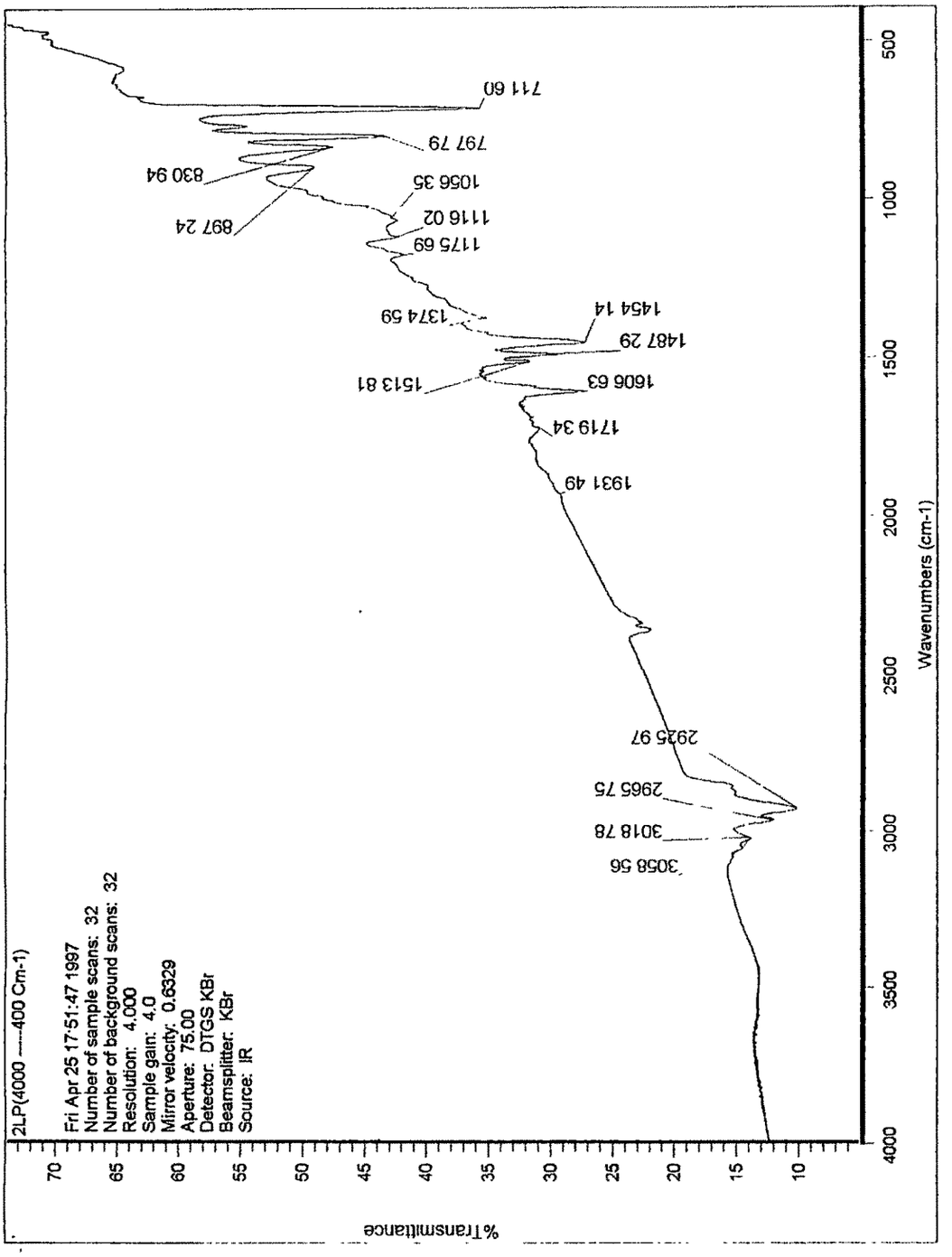

FIG. 3 5 Infrared spectra of 2P[Pd(L2AB)Cl_2]

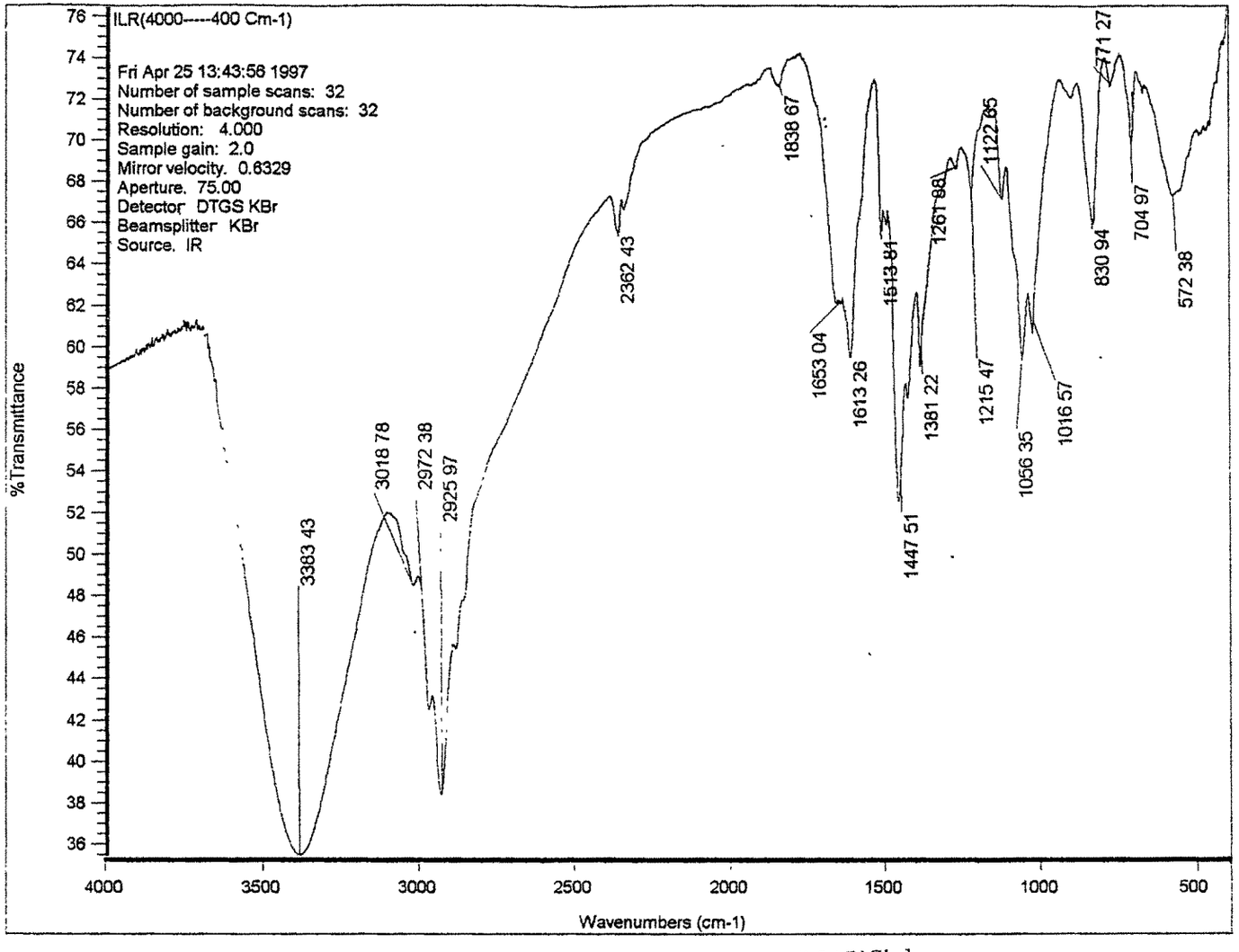

FIG. 3.6 Infrared spectra of 8P[Ru(L2AB)Cl_3]

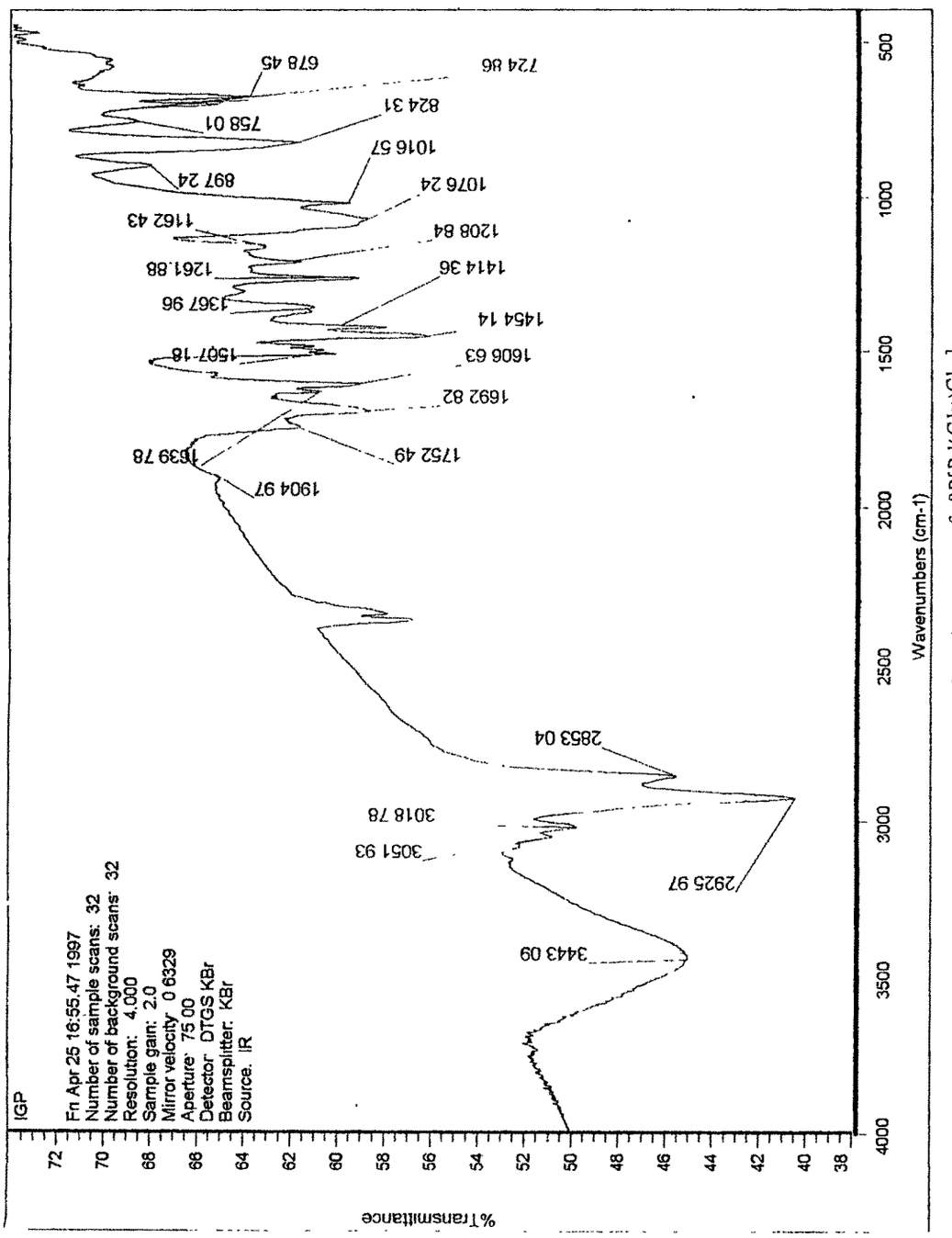

FIG. 3.7 Infrared spectra of 8P[Pd(Gly)Cl_2]

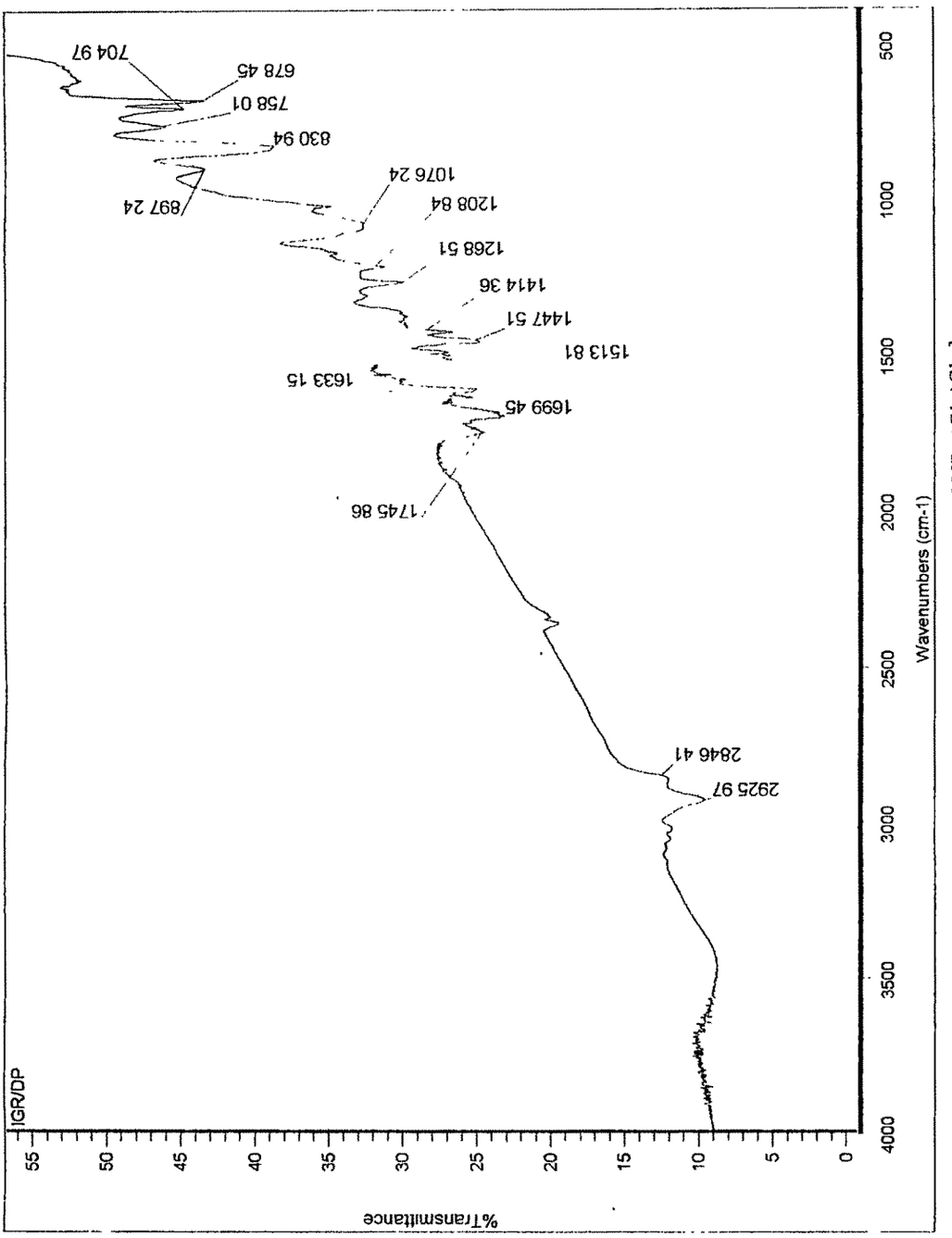

FIG. 3 8 Infrared spectra of 8P[Ru(Gly)Cl$_2$]

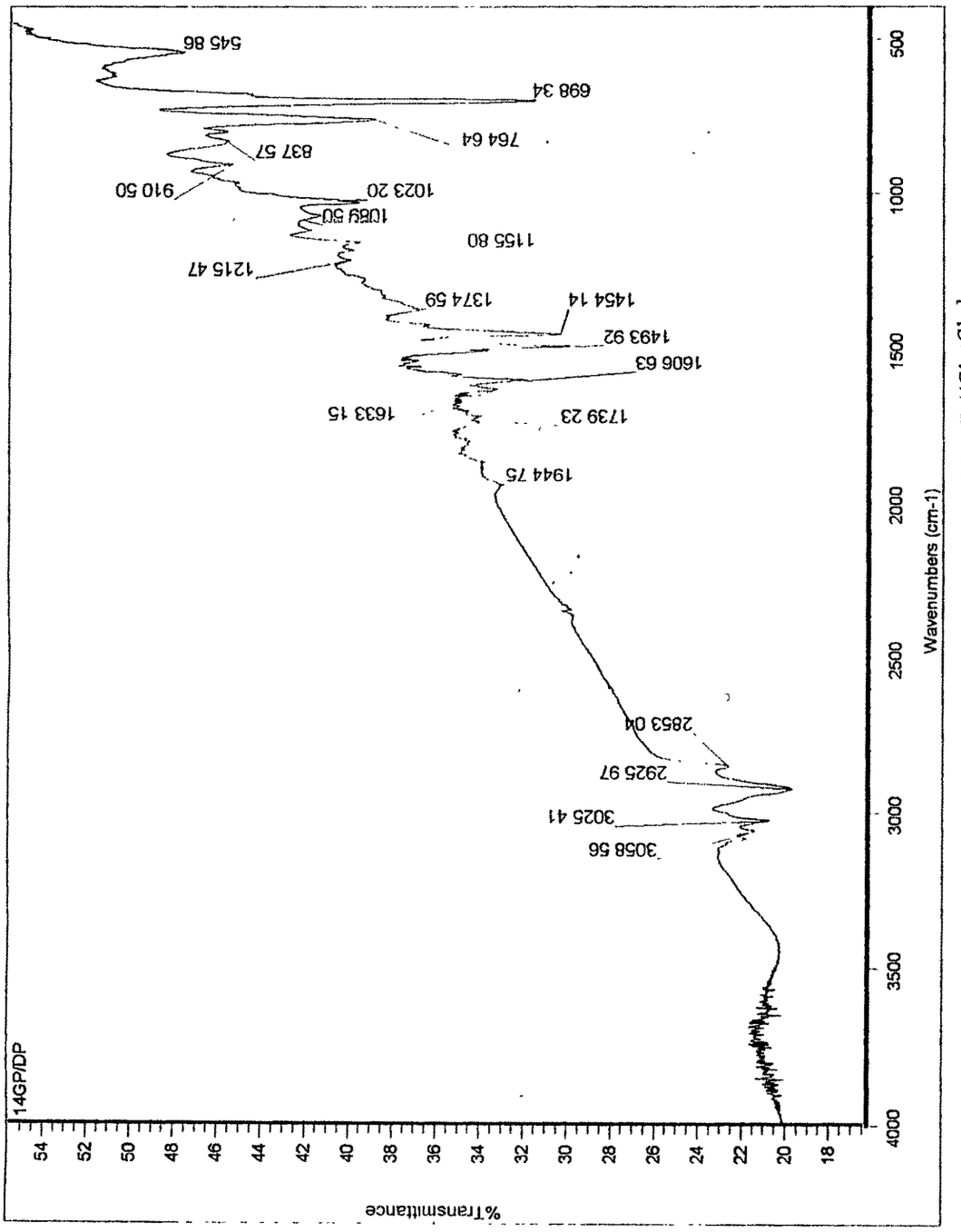

FIG. 3.9 Infrared spectra of 14P[Pd(Gly)Cl_2]

are given in Table 3.8. It is observed from the elemental analysis and metal content that all the attached ligand molecules are not involved in complex formation. Eventhen, the metal chelate formation could be concluded from the change in frequencies in absorption bands of amino group in the region of 3000 - 3400 cm^{-1} and also from appearence of new bands in the region of 1600 - 1650 cm^{-1} due to chelation

3.6.3 FTIR SPECTROSCOPY

The advantage of FTIR over disperse IR lies in the much higher signal to noise ratio which can be obtained by FT technique. The FTIR has a number of advantages over disperse-IR (13), improving the performance of IR enormously. FTIR has a strong aperture advantage because the aperture can be made larger than the corresponding slit in the monochromator. Dispersive IR spectrometers do not allow this. Thus, the quantity of light incident on the inter-ferometer is much greater than that on a monochromator. Since all signals are modulated, the effect of stray light is negligible in FTIR. Hence FTIR has emerged as a fast and sensitive technique which is well suited for catalyst studies. The FTIR spectra of the polymer supported catalysts are given in figs. 3.10 to 3.15 Table 3.9 show the FTIR frequency assignment of polymer bound ruthenium and palladium catalysts.

3.6.4 ELECTRON SPIN RESONANCE (ESR)

The electron spin resonance has been found to be a very powerful spectroscopic tool for investigating a variety of physico-chemical problem, especially when system under investigation contained a paramagnetic species. For ESR

TABLE 3.8

A summary of IR Frequency assignment for polymer bound ruthenium and palladium catalysts.

Catalyst	C - N (cm^{-1})	N - H (cm^{-1})	$-CH_2-Cl$ (cm^{-1})	-OH (cm^{-1})
2P[Ru(L2AB)Cl_3]	1062	3032 1600	1169	1679
2P[Ru(Gly.)Cl_3]	1116	3025 1606	1175	1745
8P[Ru(L2AB)Cl_3]	1056	3383 1613	1215	1653
8P[Ru(Gly)Cl_3]	1076	2925 1633	1208	1699
2P[Pd(L2AB)Cl_2]	1056	3058 1606	1175	1719
8P[Pd(L2AB)Cl_2]	1056	3396 1613	1215	1513
8P[Pd(Gly.)Cl_2]	1076	3443 1606	1162	1692
14P[Pd(L2AB)Cl_2]	1069	3085 1606	1170	1719
14P[Pd(Gly.)Cl_2]	1089	3058 1606	1215	1739

TABLE 3.9

A summary of FTIR frequency assignment for polymer bound ruthenium and palladium catalysts

Catalyst	Ru-Cl (cm^{-1})	Ru-N (cm^{-1})	Ru-O (cm^{-1})
2P[Ru(L2AB)Cl_3]	278	315	289
2P[Ru(Gly)Cl_3]	280	326	298
8P[Ru(L2AB)Cl_3]	279	315	304
8P[Ru(Gly.)Cl_3]	279	323	302
	Pd-Cl (cm^{-1})	Pd-N (cm^{-1})	Pd-O (cm^{-1})
2P[Pd(L2AB)Cl_2]	336	419	375
8P[Pd(L2AB)Cl_2]	324	420	375
8P[Pd(Gly.)Cl_2]	335	419	397
14P[Pd(L2AB)Cl_2]	325	419	376
14P[Pd(Gly)Cl_2]	325	419	383

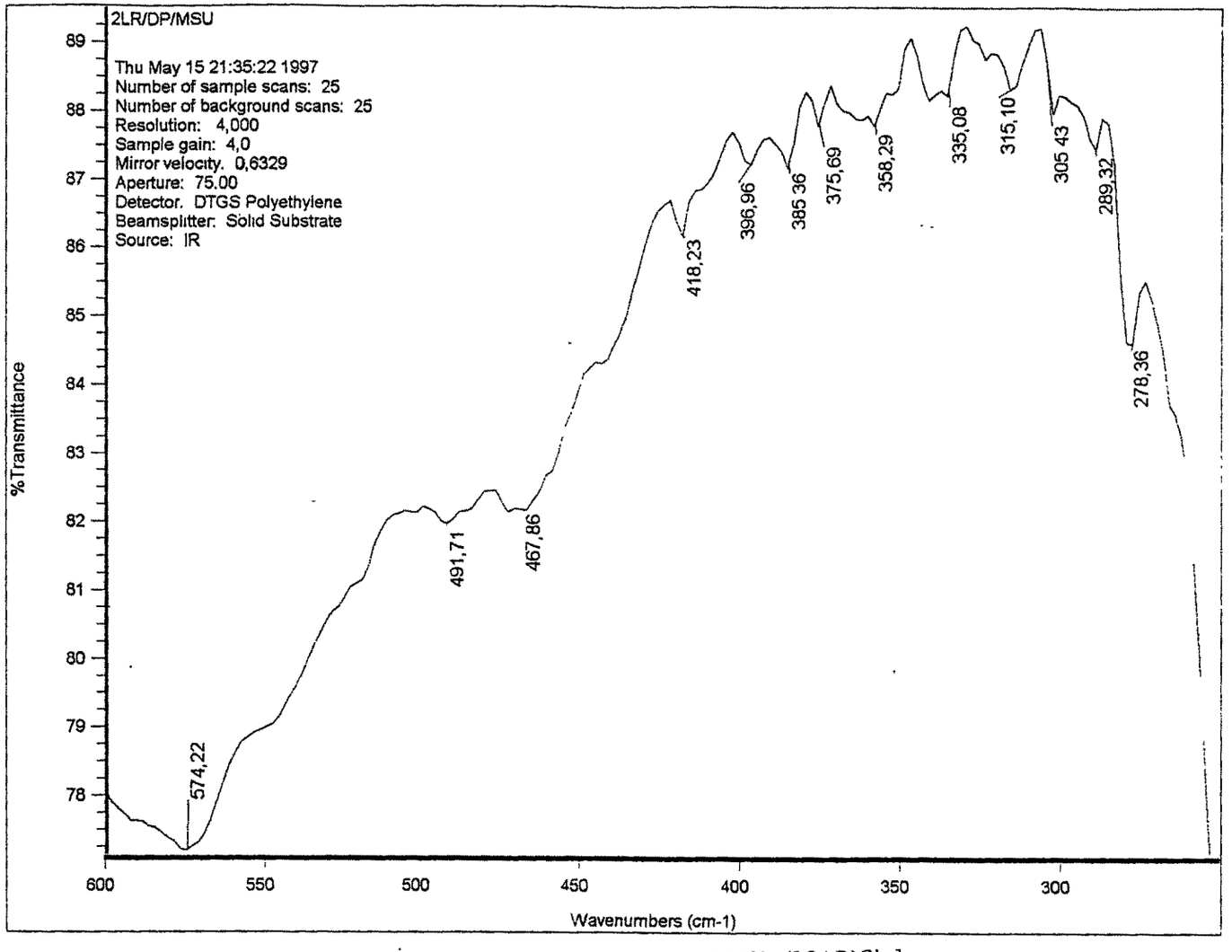

FIG. 3.10 FTIR spectra of 2P[Ru(L2AB)Cl_3]

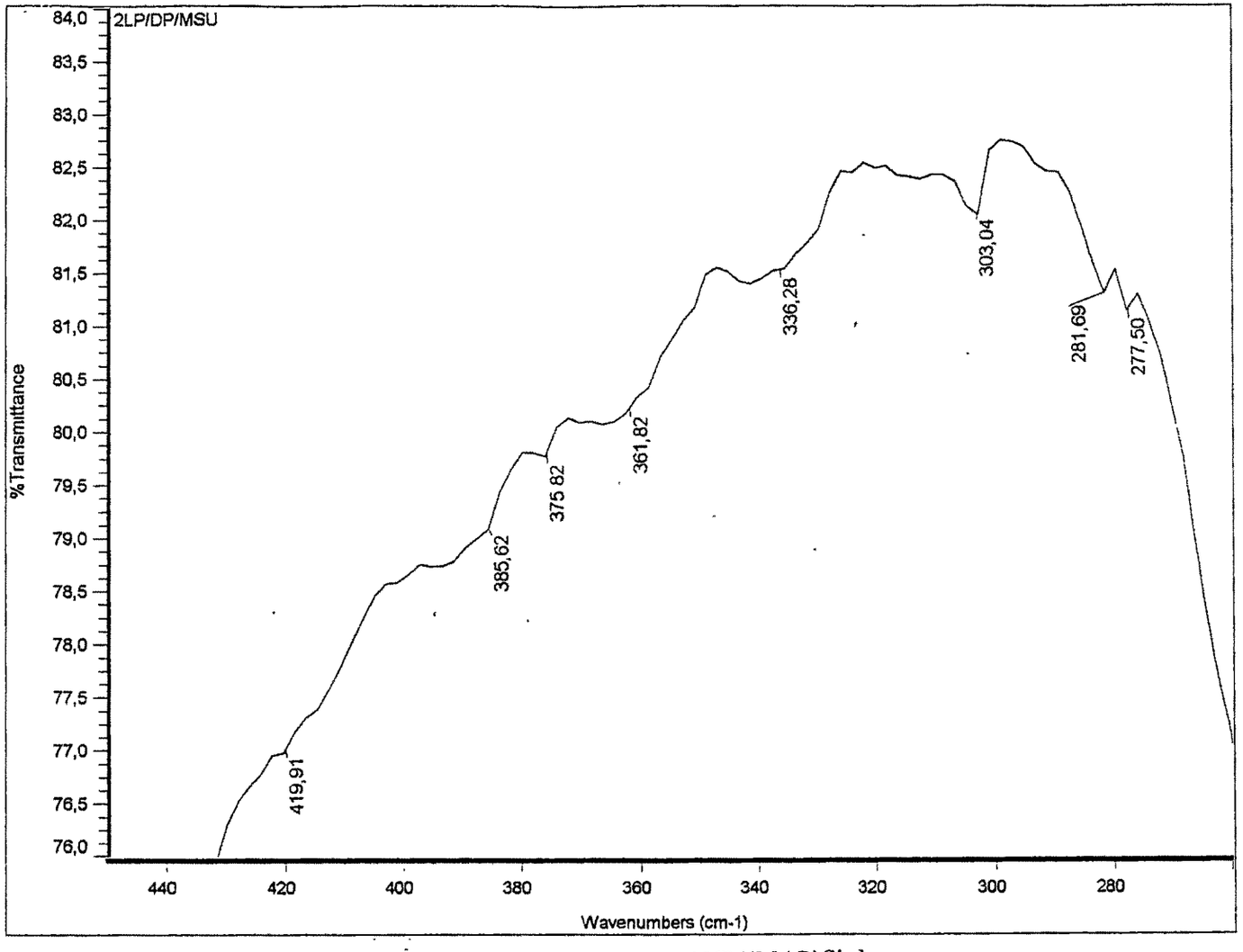

FIG. 3.11 FTIR spectra of 2P[Pd(L2AB)Cl_2]

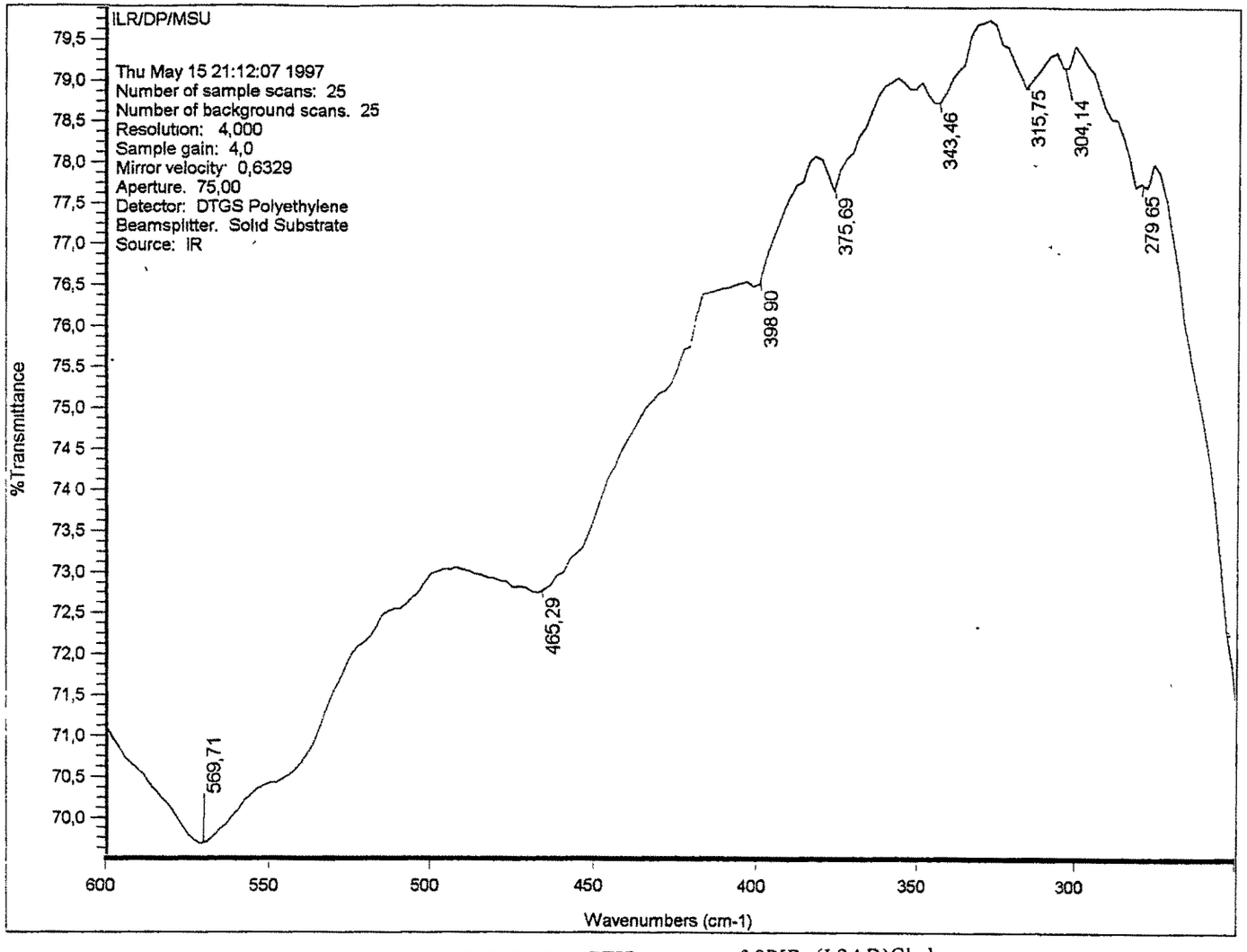

FIG. 3.12 FTIR spectra of 8P[Ru(L2AB)Cl_3]

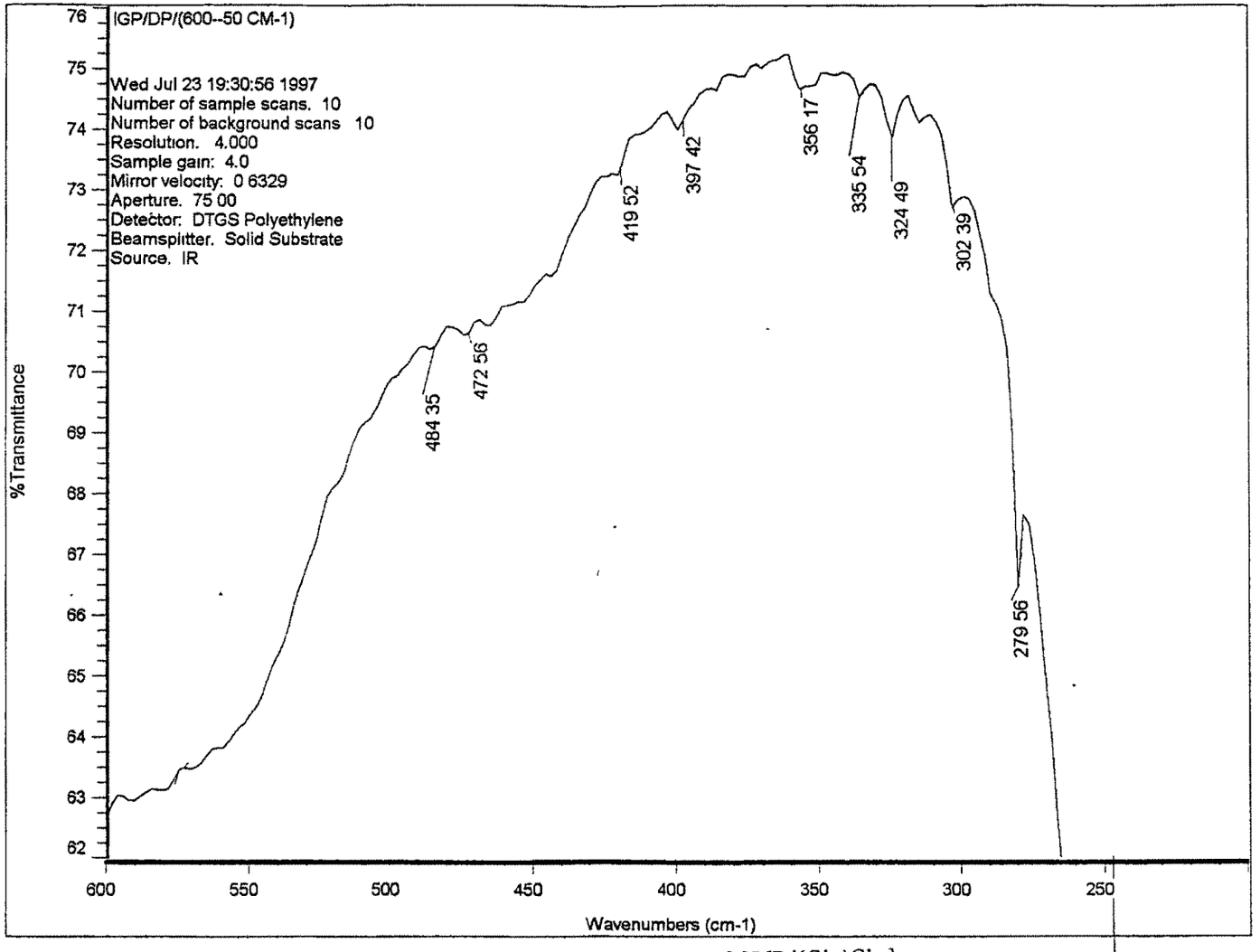

FIG 3.13 FTIR spectra of 8P[Pd(Gly)Cl_2]

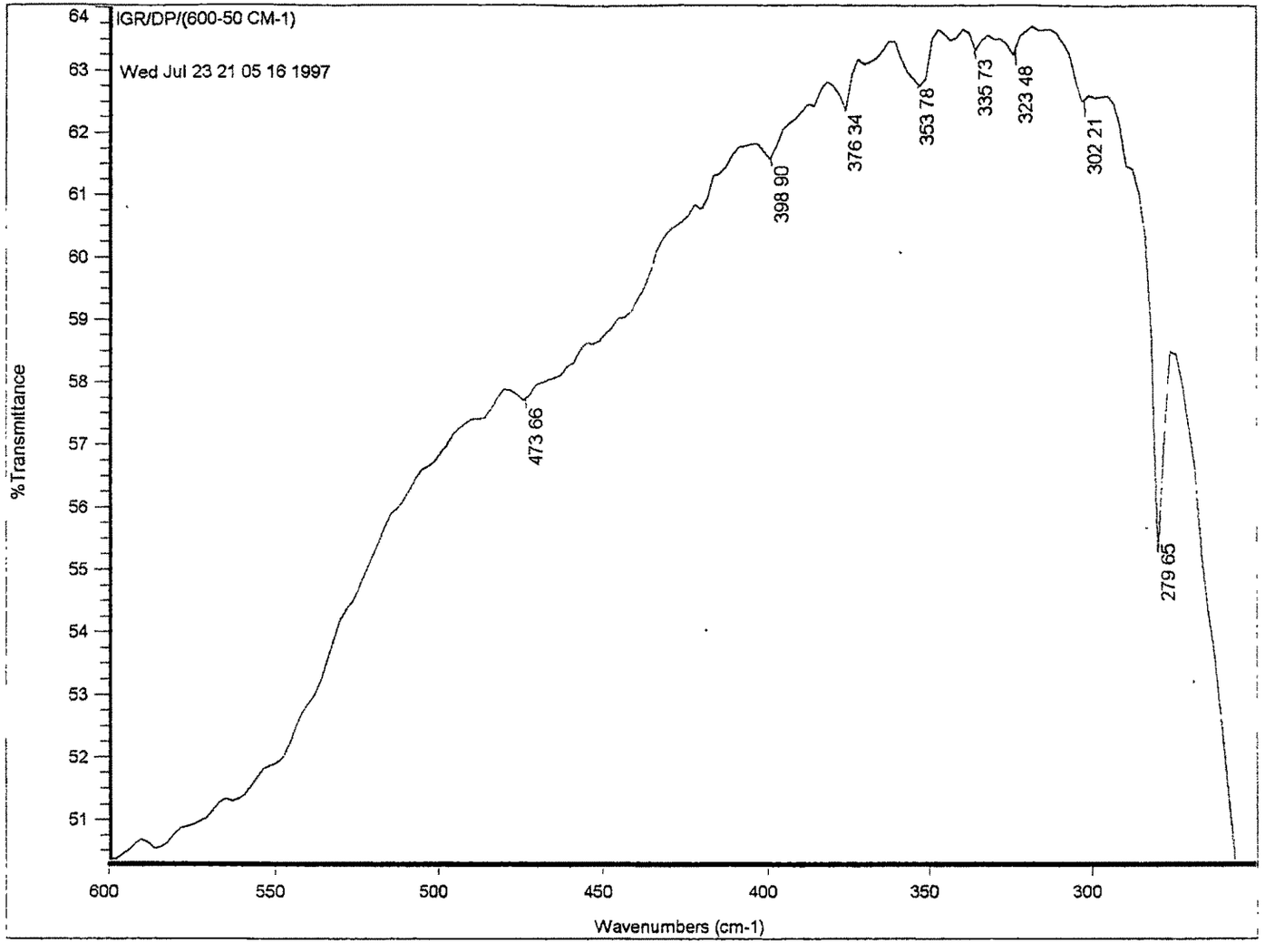

FIG. 3.14 FTIR spectra of 8P[Ru(Gly)Cl_3]

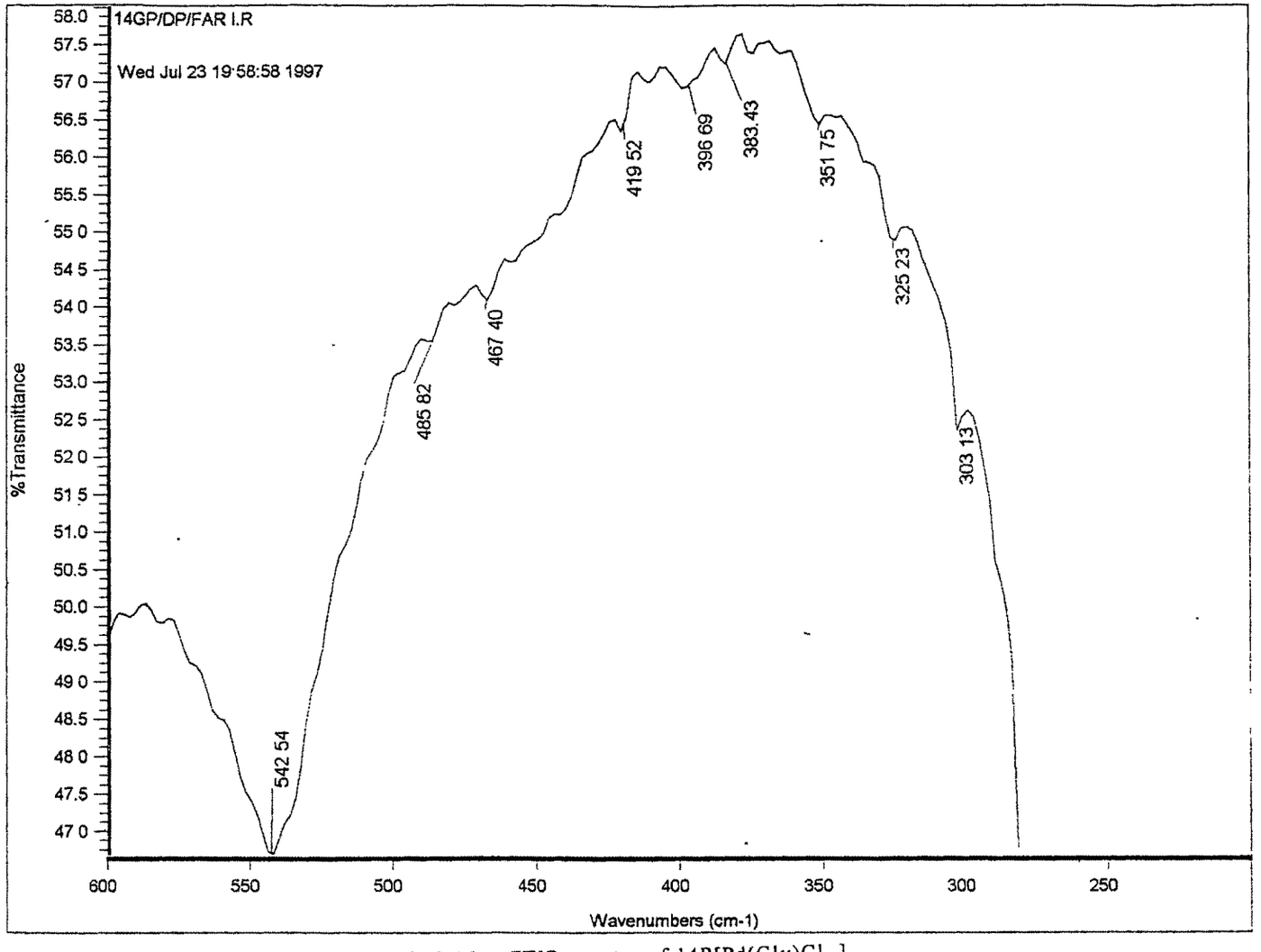

FIG. 3 15 FTIR spectra of 14P[Pd(Gly)Cl_2]

investigation, a suitable paramagnetic probe, either intrinsic or extrinsic should form a part of the system and this probe should not preferably perturb the environment. Under these conditions, the ESR spectrum of the prob gives information about the nature of chemical bonding, electron-nuclear hyperfine interactions, site symmetries and temperature or pressure included changes there in, reaction intermediates etc Therefore this technique finds wide applicability in the study of paramegnetic defects that exist on solid surface such as absorbed molecules, metal ions of d or f block element and intrinsic surface defects. The identification of the surface species has to be preceded by information on the well characterized ESR spectrum of the species of interest in bulk (14).

Transition metal ions correspond to the widest and the most fruitful field of applications of ESR spectroscopy in heterogeneous catalysis. Some well studied ions include d^1 (Ti^{+3},V^{+4},Mo^{+5}),d^3(V^{+2},Cr^{+3}),d^5(Mn^{+2},Fe^{+3},Cr^{+1}),d^7 (Co^{+2},Pd^{+3}, Rh^{+2} in low spin form) and d^9 (Cu^{+2}, Pd^{+2}, Ag^{+1}, Ni^{+2}). These studies have wide range of applications including in surface science and catalysis as the ions with these configurations give ESR spectrum over a wide range of temperature (15).

ESR is essentially due to transitions between two energy levels of an unpaired electron corresponding to two spin states in the presence of an external magnetic field. For a free electron, which is not interacting with the surrounding, the transition energy is given by

$$\nu h = \Delta E = g_e H\beta$$

Where 'h' is the plank's constant, ν is the microwave frequency, 'β' is the Bohr magneton, 'H' is the free electron with g value equal to 2.0023. In the complexes g_e varies from the free electron environment in the molecule.

ESR spectrum of catalyst 8P[Ru(Gly)Cl_3] and 14P[Pd(Gly)Cl_2] are shown in Figs. 3.16 and 3.17. The powder ESR spectrum of the 8P[Ru(Gly)Cl_3] catalyst exhibits a very weak signal at g = 1.99. The intensity of the signal must be low because of the spin lattice relaxation and broadening as is normally observed in powder spectrum. However the g value is in agreement with a low spin d^5 centre in square planar environment i.e. ruthenium is present in low spin +3 oxidation state. The possibility of Ru(II) may be eliminated because of its diamagnetic nature and hence ESR inactive. Similar results have been reported for Ru(III) carbonyl complexes (16 - 18). Taquikhan et al. have studied the ESR spectrum of Ru(III) carbonyl chelates of schiff base and from the g value it was confirmed that of ruthenium is present in +3 oxidation state (19).

The ESR spectrum of the 14P[Pd(Gly)Cl_2] catalyst exhibits an anisotropic signal at g = 4.25. This corresponds to a triplet state in Pd^{+2} with d^8 electronic configuration. This rules out the possibility of presence of Pd^{+4} which will be diamagnetic and hence ESR silent.

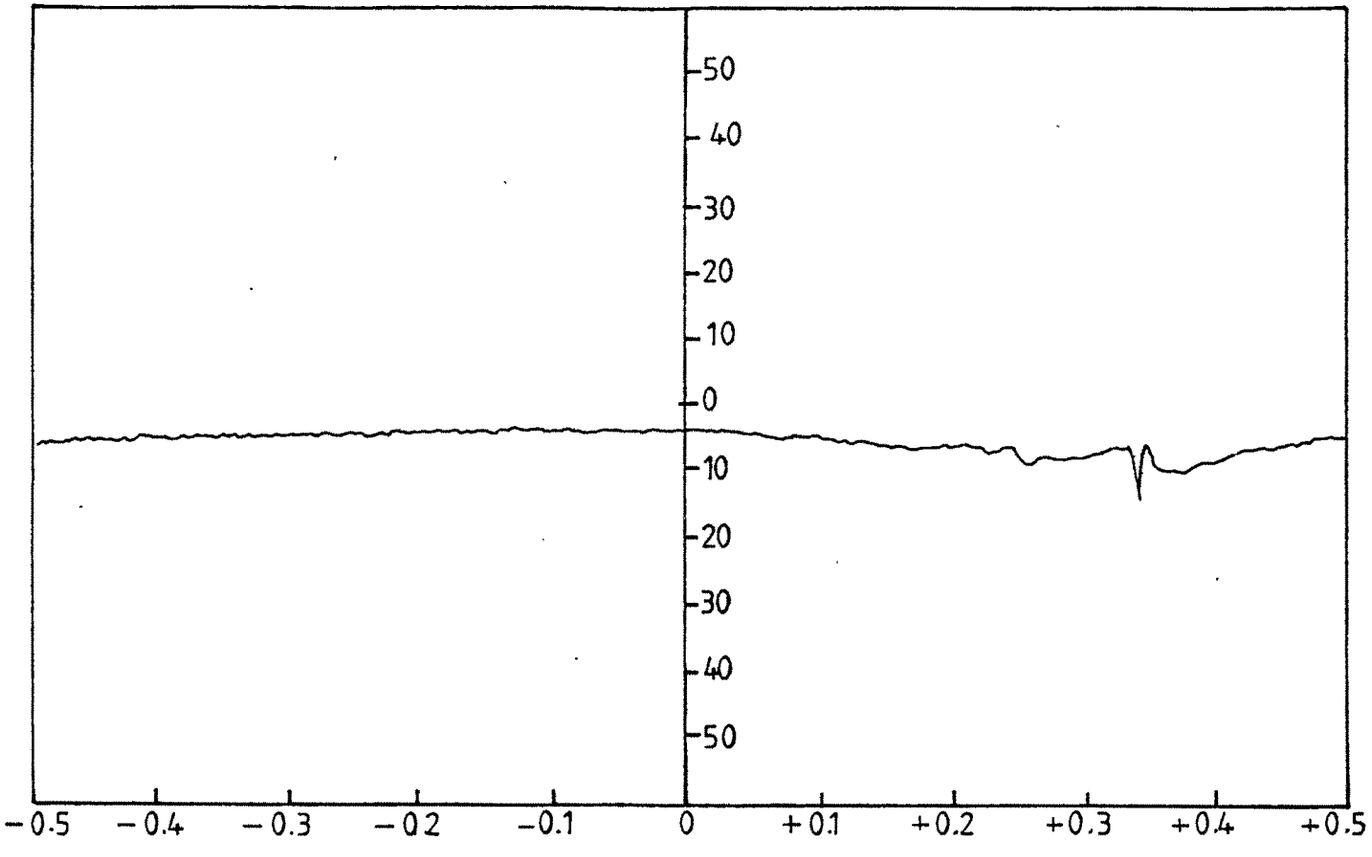

FIG. 3.16 ESR spectra of 8P[Ru(Gly)Cl_3]

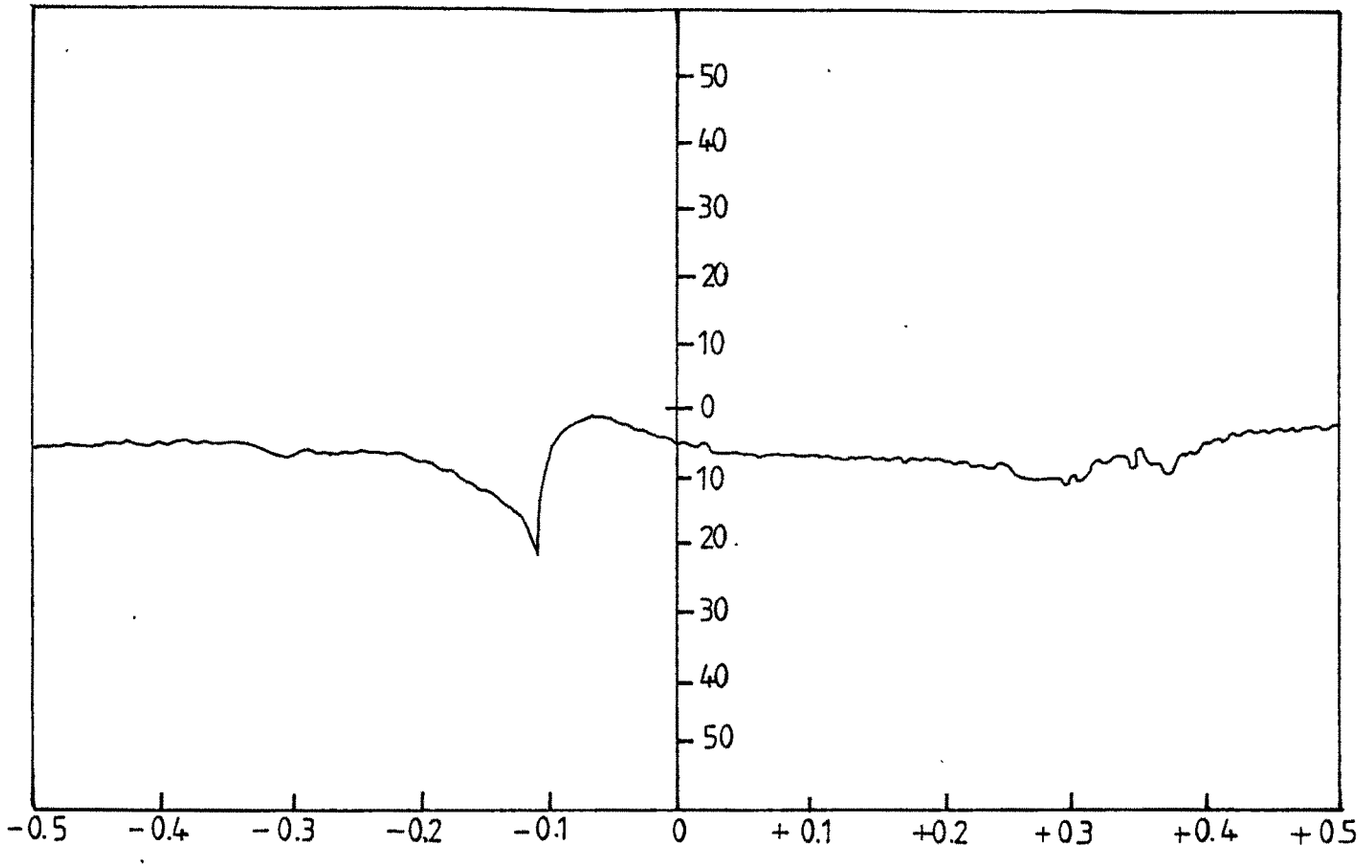

FIG. 3.17 ESR spectra of 14P[Pd(Gly)Cl_2]

3.7 MORPHOLOGY OF POLYMER SUPPORTS AND POLYMER BOUND CATALYSTS (SEM)

This technique allows essentially the imaging of the topography of a solid surface by use of back scattered or secondary electrons (20) The scanning electron microscope is especially designed for the study of bulk samples. The low energy electron (secondary electron) provides topographical contrast, allowing study of the relief of the surface, whereas the high energy (back scattered) electrons give indications about variation in mean atomic weight across the specimen surface.

The behaviour of a catalyst depends upon the structure and composition of the active component as well as the morphology of its supporting medium. It can be determined on the basis of its structure at a range of magnification (from few hundred to a few million times) which gives the information about the nature and the distribution of the active components, the nature of porosity etc. The magnification in a simple electron microscopy is limited and extension of magnification by several order of magnitude is obtained with SEM. The morphology of the catalyst can be studied with this technique (21).

Scanning electron micrographs of supports and catalysts are shown in plates 3.1 to 3.3 respectively. Comparison of micrographs of supports shows that the beads are porous and the texture changes with the change in the degree of crosslinking of polymer. Striking changes are noticed in porous texture of the polymer supports after loading the metal complexes. A change in the shape of polymer beads has been

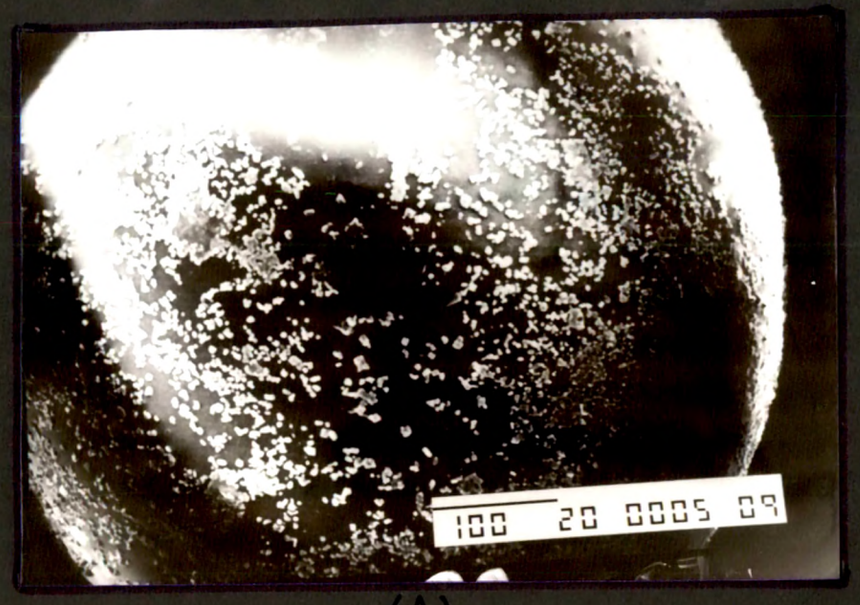

(A)

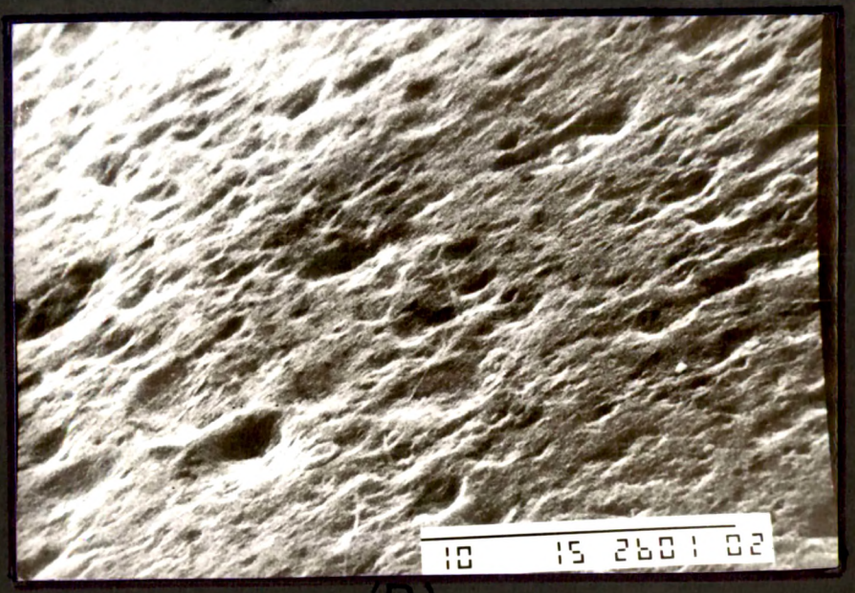

(B)

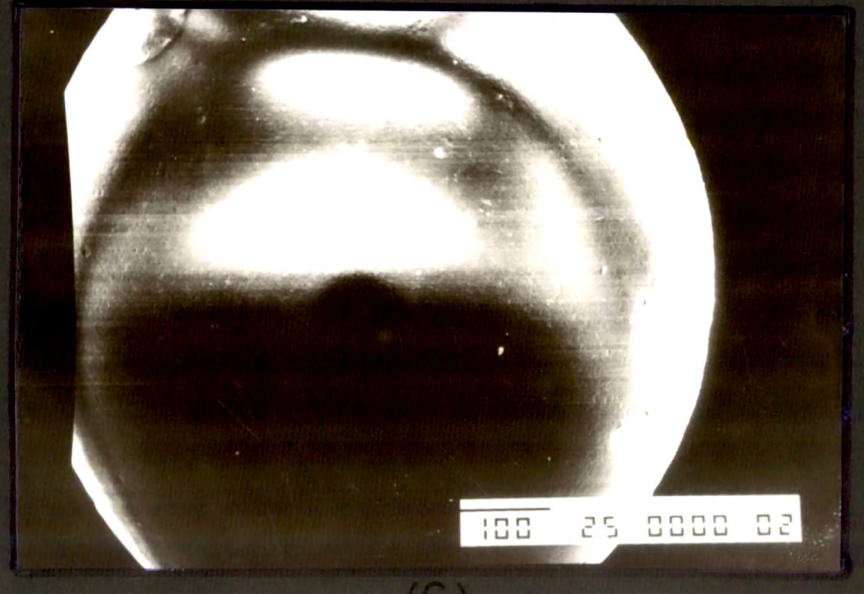

(C)

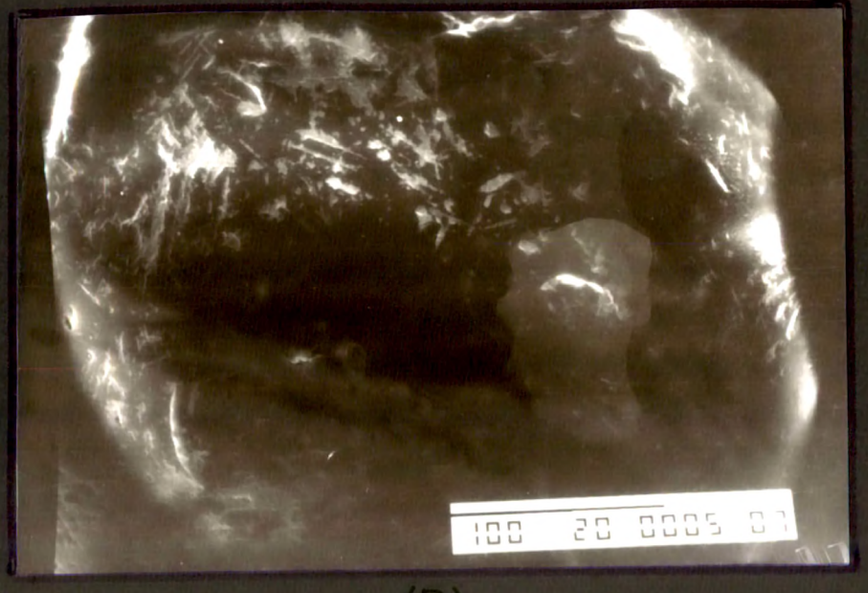

(D)

Plate 3.1 SEM of (A) 2 % support (B) 8% support
(C) 14 % support (D) 2P[Pd(L2AB)Cl_2]

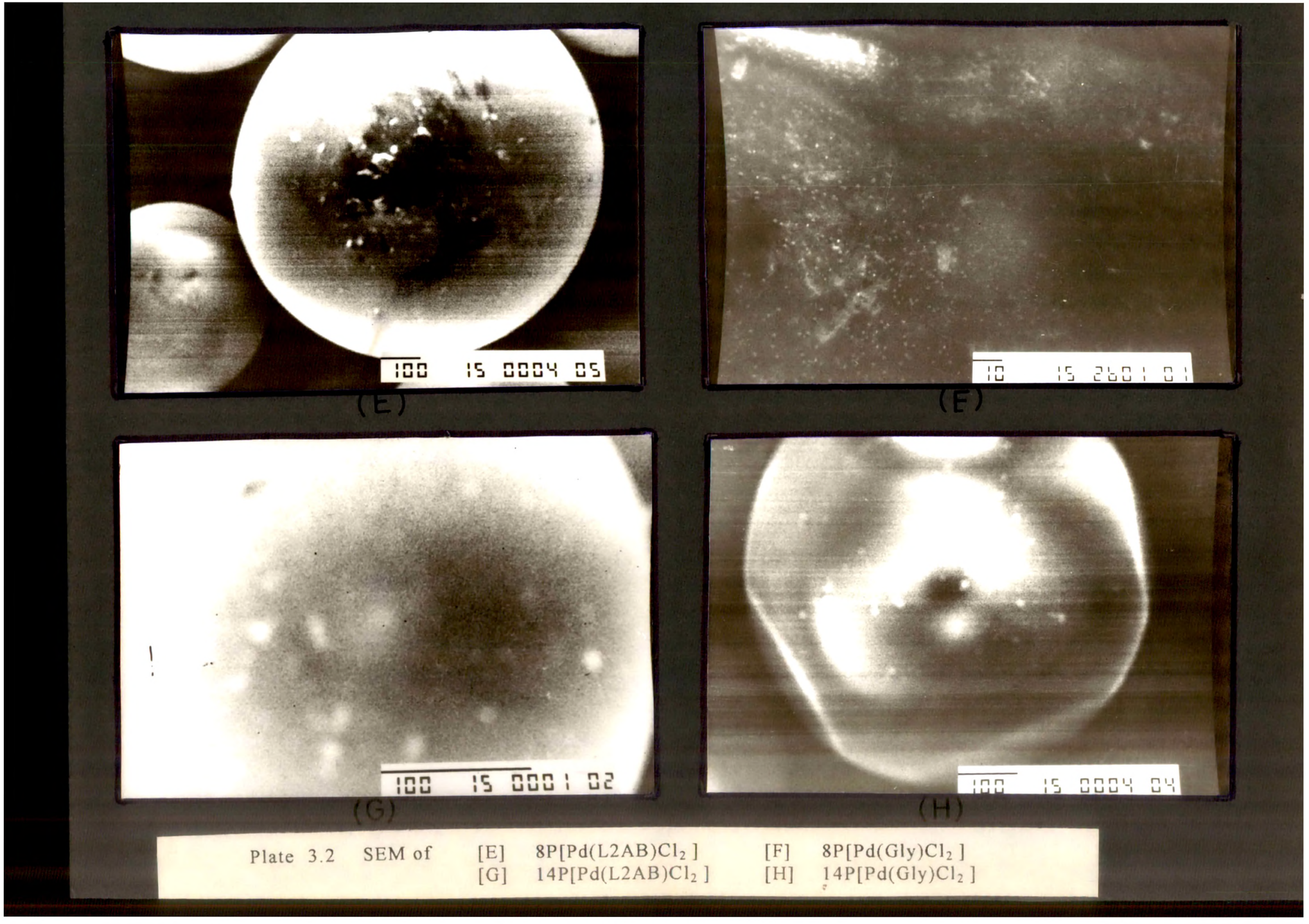

Plate 3.2 SEM of [E] 8P[Pd(L2AB)Cl_2] [F] 8P[Pd(Gly)Cl_2]
[G] 14P[Pd(L2AB)Cl_2] [H] 14P[Pd(Gly)Cl_2]

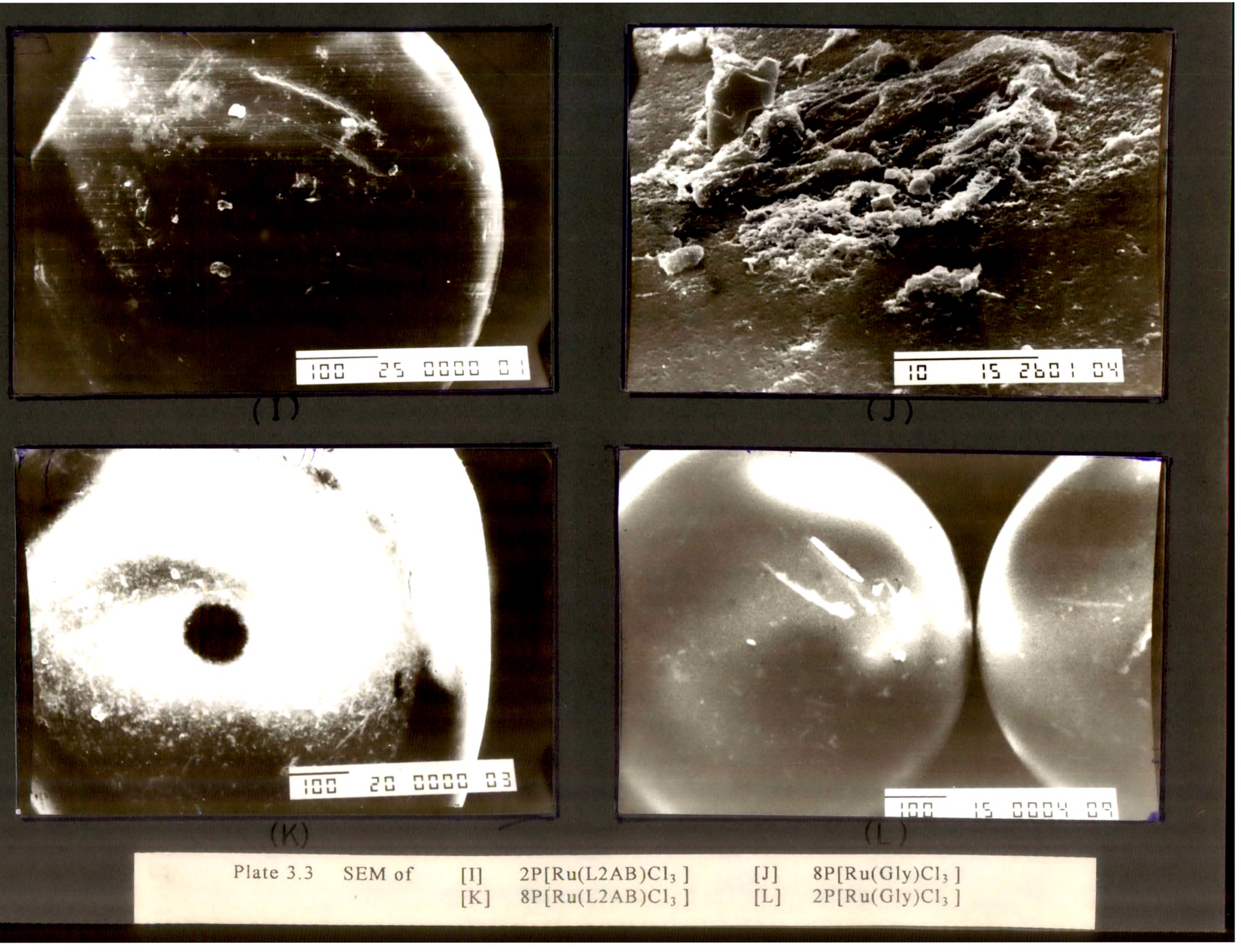

Plate 3.3 SEM of [I] $2P[Ru(L2AB)Cl_3]$ [J] $8P[Ru(Gly)Cl_3]$
[K] $8P[Ru(L2AB)Cl_3]$ [L] $2P[Ru(Gly)Cl_3]$

found after anchoring the metal complexes. These changes are also revealed in surface area measurements.

3.8 THERMAL STABILITY OF SUPPORTS AND CATALYSTS

The change in weight and thermal properties of a catalyst with changing experimental conditions can be used for a variety of studies. In the case of polymer bound metal complex catalysts, weight loss or heat change may reveal the stability and phase change as a function of environment.

The thermal stability of many metal complex catalysts was found to be enhanced when supported on inorganic oxides or polymers (22-25). Since the thermal properties and other properties of the polymer support vary with the crosslinking of the polymer, the micro environment around the metal ion changes coordination sphere of the metal ion induced by complex formation on the polymer matrix, which further leads to special stability of the metal complex. Hence the study of thermal behaviour of the polymer support and polymer bound metal complex will be useful to determine the limit of the catalytic reaction temperature.

Figs. 3.18 to 3.24 show the DTA -TG curves of the supports and the catalysts. They were found to be stable upto 140°C. However a weight loss was observed around 100°C. After that the weight loss might be due to degradation of the polymer. Thus the catalysts can be used safely upto 100°C.

From all the above physico chemical characterization and spectroscopic evidences, probable structures of the polymer bound catalysts have been proposed (scheme 3.1).

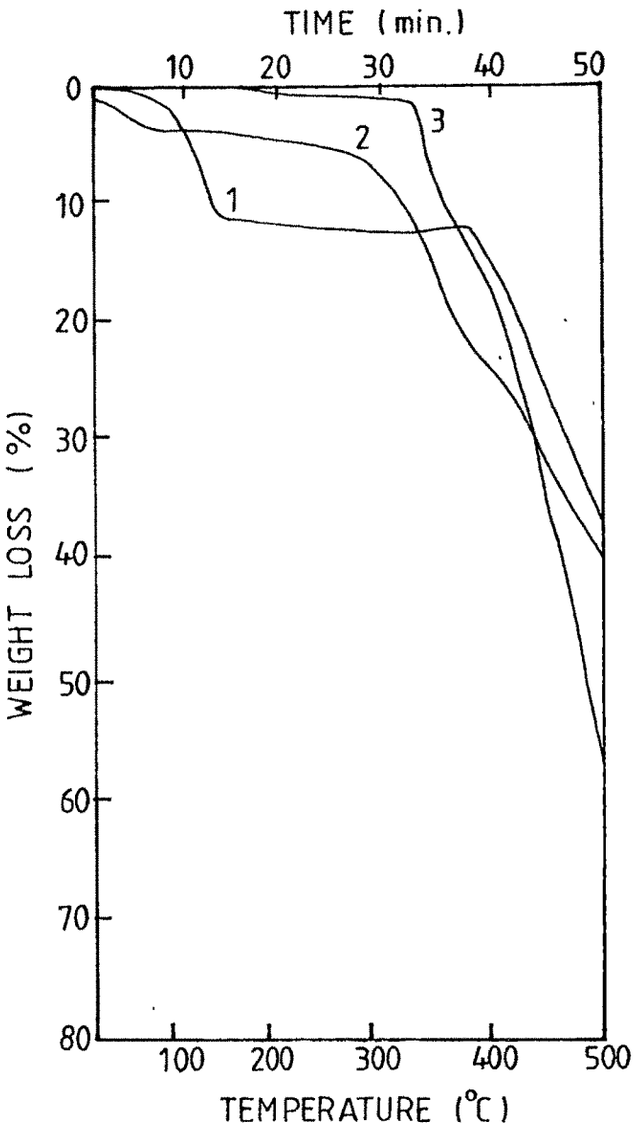

Fig. 3.18 Thermogravimetric curves of polymer supports.
(1) 2% support (2) 8% support (3) 14% support

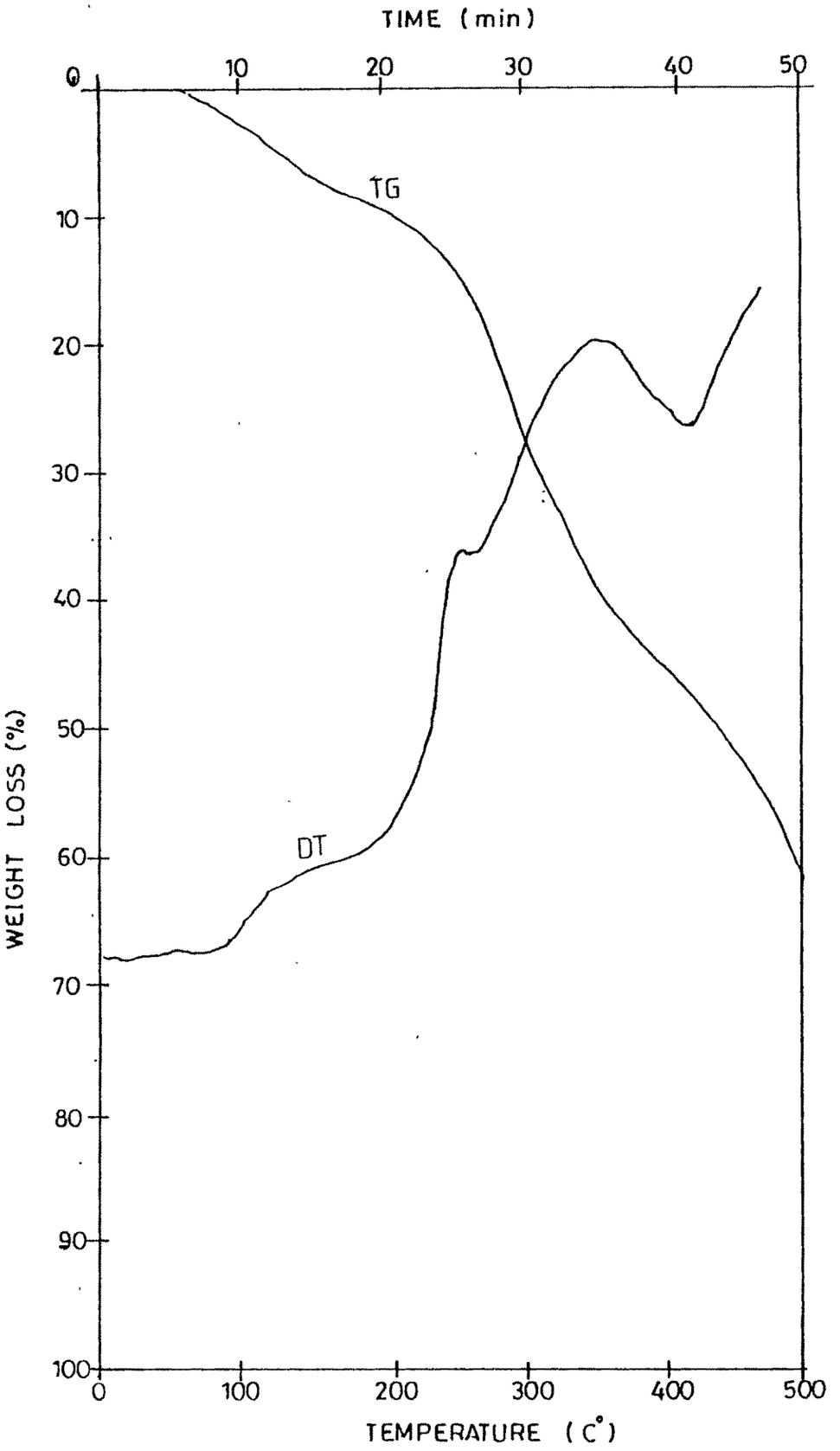

FIG. 3 19 DTA - TG Curves of 8P[Pd(L2AB)Cl_2]

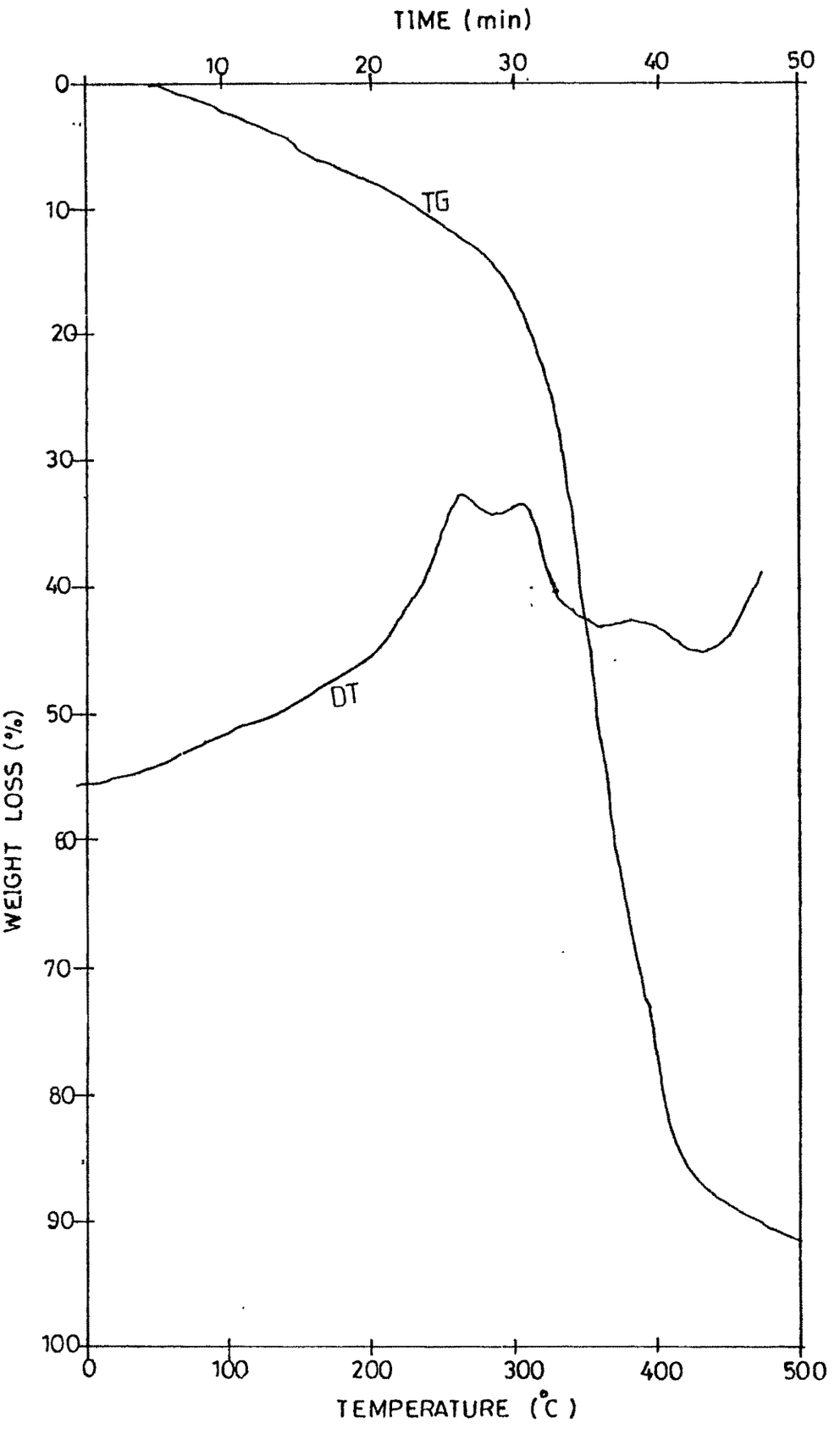

FIG. 3 20 DTA - TG Curves of 14P[Pd(L2AB)Cl_2]

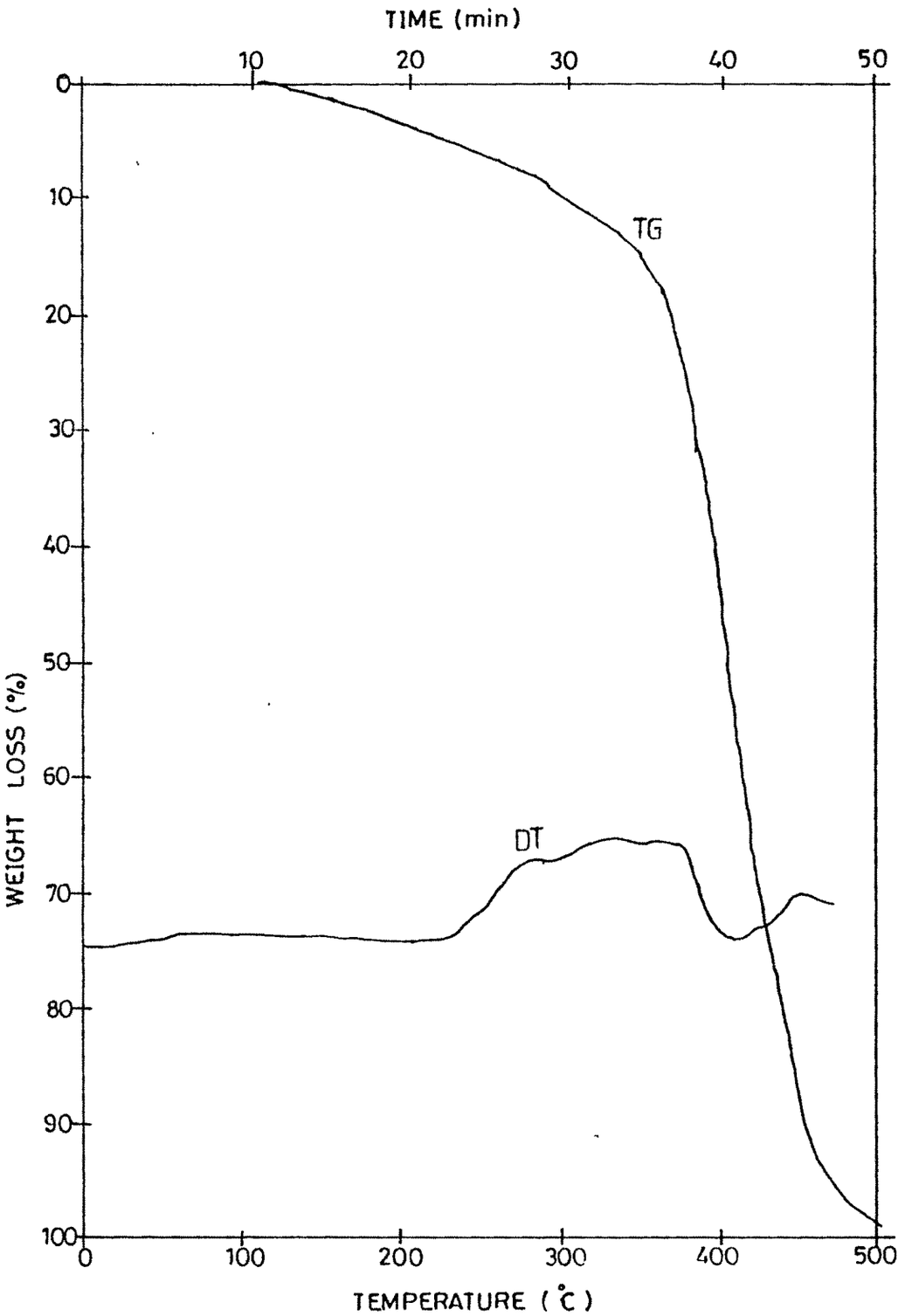

FIG. 3.21 DTA - TG Curves of 2P[Ru(Gly)Cl_3]

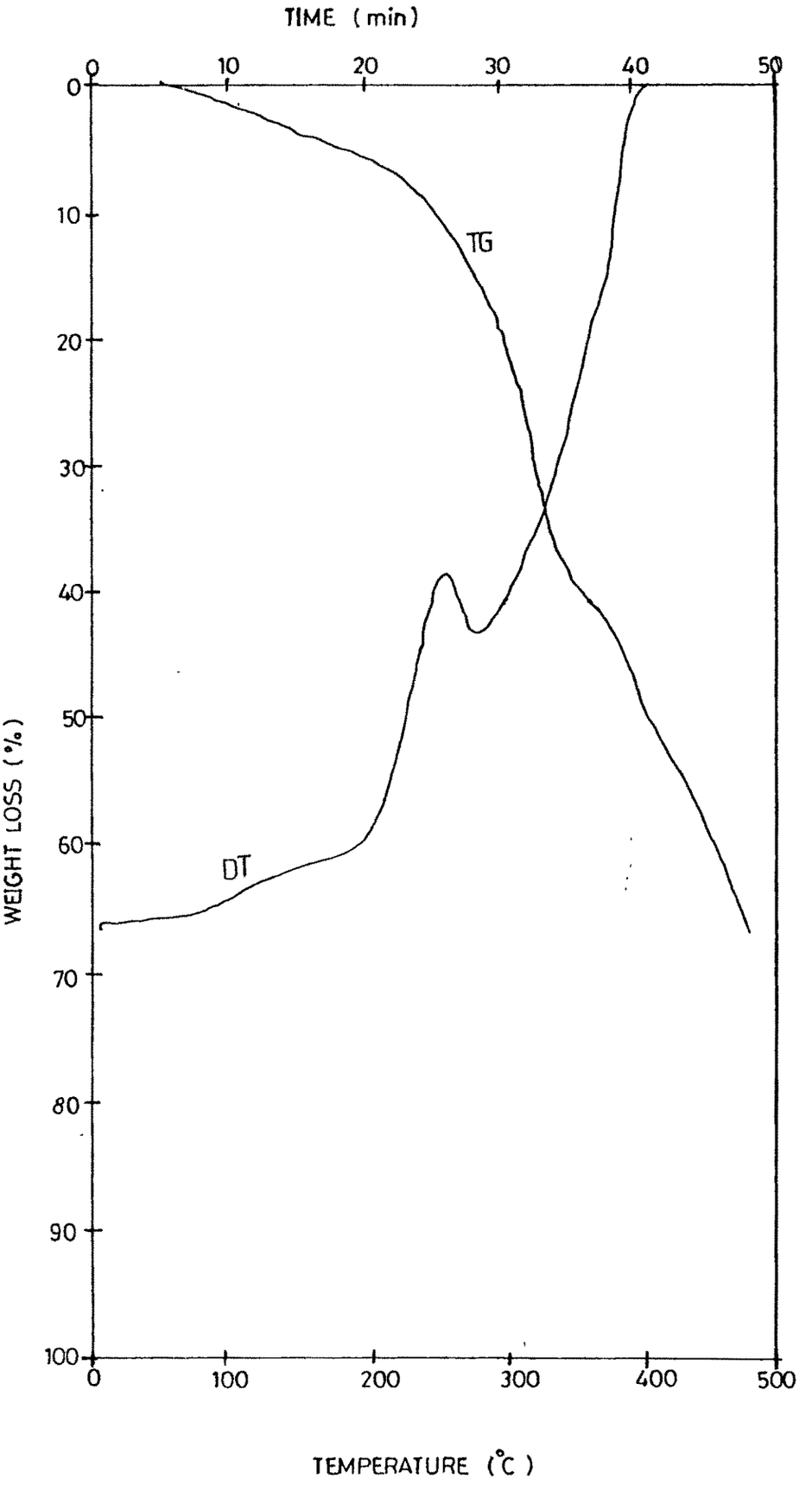

FIG. 3 22 DTA - TG Curves of 8P[Ru(Gly)Cl_3]

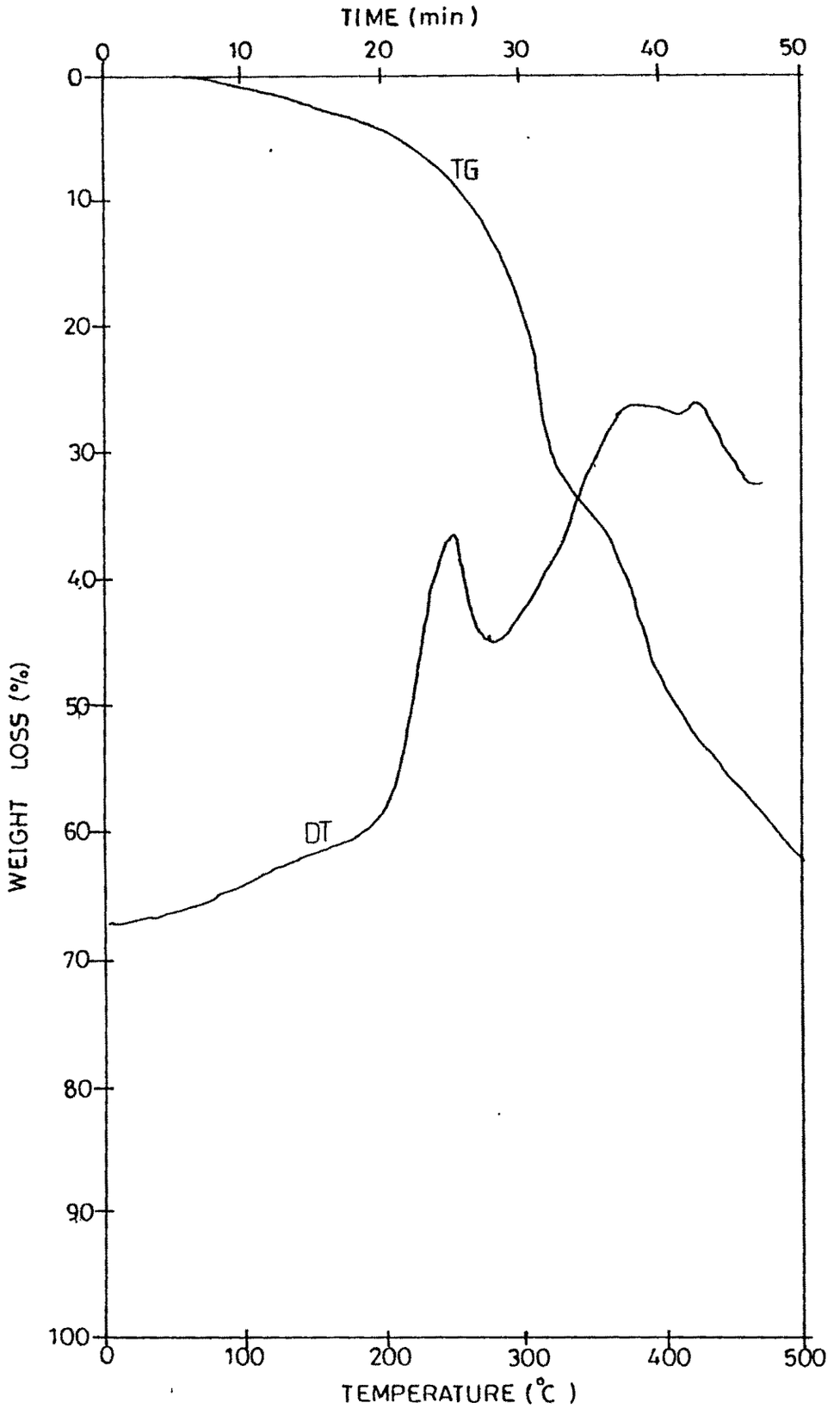

FIG. 3.23 DTA - TG Curves of 8P[Pd(Gly)Cl_2]

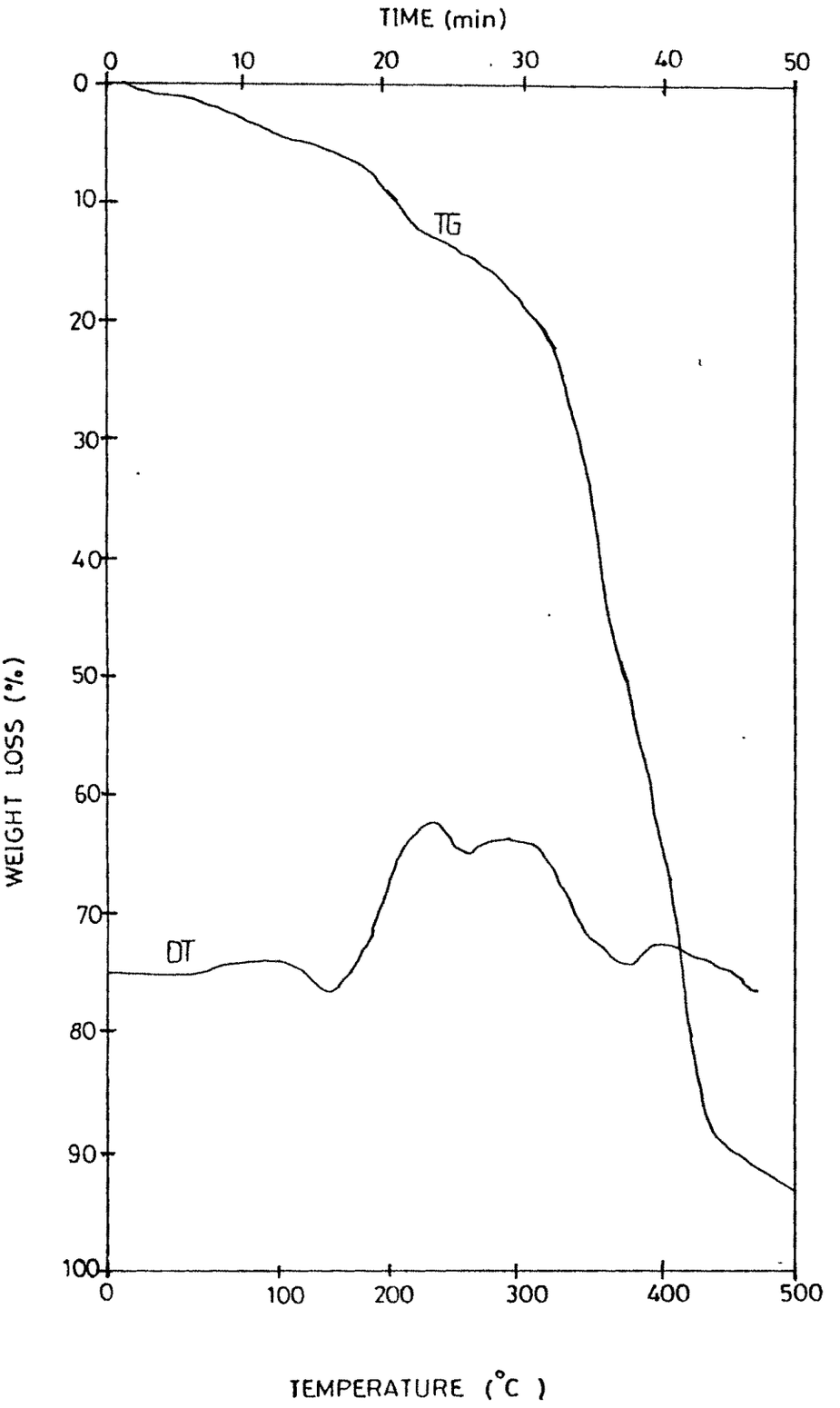

FIG 3.24 DTA - TG Curves of 14P[Pd(Gly)Cl_2]

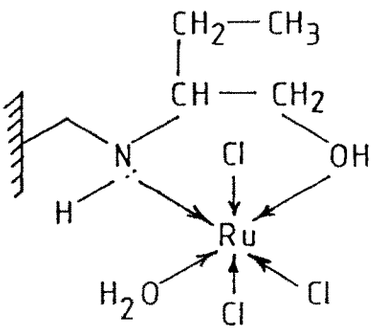

(I)

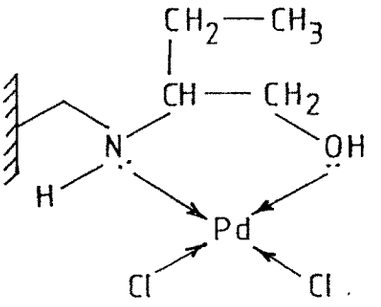

(II)

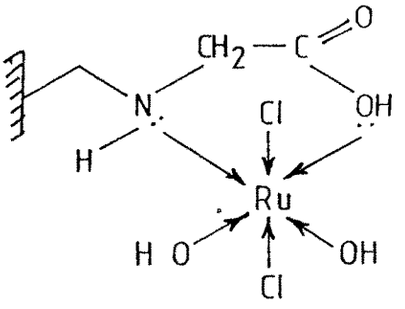

(III)

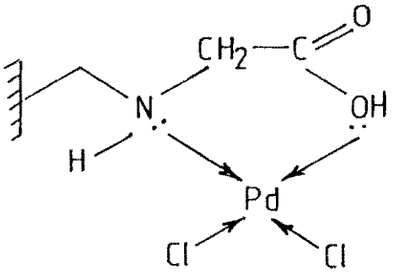

(IV)

(SCHEME - 3.1)

3.9 REFERENCES

1. F.W.Billmeyer, " Textbook of Polymer Science", Wiley Inter Science, New York, Third edition (1979).
2. R. B. Seymour " Introduction of Polymer Chemistry " McGraw-Hill, New York (1971).
3. R. Kumin " Ion Exchange Resins " john Wiley and sons Ltd. (1958).
4. D. M. Yoing and A. D. Crowell " Physical Adsorption of gases" Butter worths, London (1962).
5. S. J. Gregg and K. S. W. Sing "Adsorption, Surface and Porosity " Academic press, London (1967).
6. K. Klier, Catal. Rev. (1967) 207.
7. G. Kortum " Reflectance Spectroscopy, Principles, Methods and Applications" Springer-Verlag, Berlin (1969).
8. W. N. Delgass, G. L. Haller, R. Kellerman and J. H. Lunsford "Spectroscopy in Heterogeneous Catalysis " Academic press, New York (1979).
9. W.W. Wendlandt and H. G. Hecht " Reflectance spectroscopy " Wiley Inter. Sci., New York (1966).
10. Y. Kurimuka, E. Isuchida and M. Kaneho, J. Poly. Sci., 9(1971) 352.
11. J. Roda, Macromol. Chem., 178 (1971)203.
12. J. John, Ph.D Thesis, M S. University of Baroda (1993).
13. B. A. Goodman and J. B. Raynor, Adv. Inorg. Chem., Radio Chem., 13 (1979) 175.
14. J. Reed, P. Eisenberger, B. K. Teo and B. M. Kincaid, J. Am. Chem. Soc., 100 (1978) 2375.
15. M S. Sastry in " Spectroscopy methods in Heterogeneous catalysis " Ed. by N. M. Gupta, V. B. Kartha and R. A

Rajadhyasha, Tata McGraw-Hill Pub. Ltd., New Delhi, India (1991).

16. A. Hudson and M. J. Kennedy, J. Chem. Soc. (1969) 1169.
17. B. L. Gustafson, M. J. Lin and J. H. Lunsford, J. Phys. Chem., 84 (1980) 3211.
18. S. Sasaki, Y. Yanase, N. Hagiwara, T. Takeshila, H. Naganuma, A. Ohyoshi and K. Ohkubo, J. Phys. Chem. Soc., 86 (1982) 1038.
19. M. M. Taquikhan, D. Srinivas, R. I. Kureshy and N. H. Khan, Inorg. Chem., 29 (1990) 2330.
20. J. I. Goldstein and H. Yakowitz, Eds. " Practical Scanning Electron " Plenum press, New York (1975).
21. J. V. Sanders in "Catalysis, Science and Technology " Eds. J.R. Anderson and M. bondart, Springer-Verlag, Berlin Heidelberg, 7(1985) 51.
22. L Jinxing, Y. Lixin, G. Shivrying, H. Lijuan, I. Renyuam and L. Dongbai, Thermochemica Acta., 123 (1988) 121.
23. N. L. Holy, J. Org. Chem., 44 (1979) 239.
24. N. L. Holy in " Fundamental Research in Homogeneous Catalysts " Ed. M. Isutsui, Plenum Press, New York (1979) 691.
25. J. Sestak, V. Satara and W. W. Wendlandt, Thermochim. Acta., 7(1973) 333.